ESR analyses of picket fence Mn^II and 6th ligand coordinated Fe^III porphyrins (S = 5/2) and a Co^II(hfac) complex (S = 3/2) with sizable ZFS parameters revisited: A full spin Hamiltonian approach and quantum chemical calculations

ESR analyses of picket fence Mn^{II} and 6th ligand coordinated Fe^{III} porphyrins (S = 5/2) and a Co^{II}(hfac) complex (S = 3/2) with sizable ZFS parameters revisited: A full spin Hamiltonian approach and quantum chemical calculations

Takeshi Yamane, Kenji Sugisaki, Hideto Matsuoka, Kazunobu Sato, Kazuo Toyota, Daisuke Shiomi, Takeji Takui

Citation	Dalton Transactions, 47(46); 16429-16444
Issue Date	2018-12-14
Type	Journal Article
Textversion	Author
Relation	The following article has been accepted by Dalton Transactions. After it is published, it will be found at https://doi.org/10.1039/C8DT02988A.
DOI	10.1039/C8DT02988A

YAMANE, T., SUGISAKI, K., MATSUOKA, H., SATO, K., TOYOTA, K., SHIOMI, D., & TAKUI, T. (2018). ESR analyses of picket fence Mn^{II} and 6th ligand coordinated Fe^{III} porphyrins (S = 5/2) and a Co^{II}(hfac) complex (S = 3/2) with sizable ZFS parameters revisited: a full spin Hamiltonian approach and quantum chemical calculations. *Dalton Transactions*. 47, 16429-16444. doi:10.1039/C8DT02988A

Journal Name

ARTICLE

ESR analyses of picket fence Mn^{II} and 6th ligand coordinated Fe^{III} porphyrins (S = 5/2) and a Co^{II}(hfac) complex (S = 3/2) with sizable ZFS parameters revisited: A full spin Hamiltonian approach and quantum chemical calculations

Received 00th January 20xx,
Accepted 00th January 20xx

DOI: 10.1039/c8dt02988a

www.rsc.org/

Takeshi Yamane,[a] Kenji Sugisaki,[a] Hideto Matsuoka,[a] Kazunobu Sato,*[a] Kazuo Toyota,[a] Daisuke Shiomi[a] and Takeji Takui*[a,b]

The fictitious spin-1/2 (effective spin-1/2) spin Hamiltonian approach is the putative method to analyze the conventional fine-structure/hyperfine ESR spectra of high spin metallocomplexes with sizable zero-field splitting (ZFS) tensors since early in 1950's, and the approach gives salient principal g^{eff}-values far from g = 2 without explicitly affording their ZFS values in most cases. The experimental g^{eff}-values thus determined, however, never agree with those (g^{true}-values) of the true principal **g**-tensors, which are obtainable form reliable quantum chemical calculations. We have recently derived exact or extremely accurate analytical expressions for the g^{eff}/g^{true} relationships for the spin quantum number S's up to S = 7/2: T. Yamane, et al., *Phys. Chem. Chem. Phys.*, 2017, **19**, 24769–24791. In this work, we have removed the limitation of the collinearity between **g**- and ZFS tensors and derived the generalized g^{eff}/g^{true} relationships. To illustrate the usefulness of the present approach, we have revisited important typical high spin systems with large ZFS values such as picket fence metalloporphyrins with Mn^{II} (S = 5/2) (Q. Yu, et al., *Dalton Trans.*, 2015, **44**, 9382–9390), a 6th ligand coordinated porphyrin with Fe^{III} (S = 5/2) (Y. Ide, et al., *Dalton Trans.*, 2017, **46**, 242–249) and a pseudo-octahedral Co^{II} (S = 3/2)(*hfac*)$_2$ complex (D. V. Korchagin, et al., *Dalton Trans.*, 2017, **46**, 7540–7548), completing the ESR spectral and magnetic susceptibility analyses and gaining significant physical insights into their electronic structures. The off-principal axis extra peaks overlooked in the documented spectra of the picket fence Mn^{II} porphyrins have fully been assigned, affording their accurate true **g**-, hyperfine and ZFS tensors, for the first time. For the Co^{II} complex, the occurrence of the non-collinearity between the **g**- and ZFS tensors has been discussed by using the generalized g^{eff}/g^{true} relationships. We have attempted to carry out reliable DFT-based and *ab initio* quantum chemical calculations of their magnetic tensors, in which spin–orbit couplings are incorporated, reproducing the experimental true tensors. We emphasize that the incorporation of multi-reference nature in the electron configuration is important to interpret the magnetic tensors for the Co^{II} complex.

Introduction

Electronic high spin states originating in open shell metal ions in chemical entities can typically be seen in synthetic metallocomplexes with biological implications or new molecular functionalities, and widely seen in biological systems such as metalloproteins.[1–3] Their magnetic properties feature in sizable zero-filed splitting (ZFS) tensors ranging from a few tenths to hundreds of cm^{-1}, which are mainly governed by spin–orbit couplings intrinsic to heavy elements and their relativistic effects. Noticeably, recent advance in molecular materials science relevant to high blocking temperature characterizing single molecule magnets (SMM's) or single ion magnets suggests that tuning of the spin–orbit couplings is essentially important. Another example is seen in the molecular design/molecular optimization for molecular spin qubits or ensemble high spin systems as quantum spin memory devices. The tuning of ZFS parameters is also essential for the spin memory device to couple with superconducting flux qubits or with planar cavity modes.[4,5] These examples imply that practical guidelines to design and synthesize high spin metallocomplexes, whose molecular functionalities are dominated by the spin–orbit couplings, make important contributions to the emerging field from the chemistry viewpoint.

From the theoretical viewpoint, reliable quantum chemical calculations of open shell metallocomplexes with sizable molecular structures are emerging in order to interpret their experimental magnetic parameters including the sizable ZFS tensors.[6,7] Until now theoretical calculations of ZFS tensors for complex antiferromagnetically coupled spin systems such as Mn clusters are intractable and only a few reports based on DFT for

[a] Department of Chemistry and Molecular Materials Science, Graduate School of Science, Osaka City University, 3-3-138, Sugimoto, Sumiyoshi, Osaka, 558-8585, Japan.
[b] Support Department/University Research Administrator Center, University Administration Division, Osaka City University, 3-3-138, Sugimoto, Sumiyoshi, Osaka 558-8585, Japan.

† Electronic Supplementary Information (ESI) available: Derivations of the g^{eff}/g^{true} relationships based on the exact analytical and genuine Zeeman perturbation treatments, the simulated ESR spectra and details of quantum chemical calculations for the magnetic tensors. See DOI: 10.1039/c8dt02988a

the clusters have been documented,[8–10] and needless to say that broken-symmetry DFT calculations for ZFS tensors are still problematic from a theoretical viewpoint. Thus, it is of essential importance to experimentally determine the true **g**- and ZFS tensors of high spin complexes and to compare them with theoretical tensors. Experimental determination of the principal axes of the magnetic tensors gives a key for some cases with extremely asymmetric ZFS tensors.[11] Only the true **g**-tensors deserve the comparison with quantum chemical calculations, giving more significant physical insights into the electronic structures of high spin metallocomplexes than those so far obtained in terms of traditional ligand field treatments.

As well known, the fictitious spin-1/2 (effective spin-1/2) spin Hamiltonian approach is the putative method to analyze the conventional fine-structure/hyperfine ESR spectra of high spin metallocomplexes with sizable ZFS tensors since early in 1950's, and the approach gives salient principal g^{eff}-values far from g = 2 without explicitly affording their ZFS values in most cases. We note that the approaches have been in good harmony with advance in ligand field theory,[12–15] prior to the appearance of sophisticated quantum chemical calculations. Particularly, in the case that the systems under study undergo the significant departure from the axial symmetry of their ZFS tensor, as stated above, the unexpected variation of the g^{eff}-values occurs for half-integer high spins. Naturally, the experimental g^{eff}-values thus determined never agree with those (g^{true}-values) of the true principal **g**-tensors in a straightforward manner, which are obtainable from reliable quantum chemical calculations. Clear differentiation between the two values seems important to quantitatively interpret the electronic structures of high spin metallocomplexes in terms of quantum chemistry, or to tune the spin–orbit couplings by invoking molecular optimization in synthetic strategy. We emphasize that Co^{II} complexes in relatively low symmetric environment give a testing ground for the validity of the ligand field theory combined with spin–orbit couplings and full configuration interactions within d electrons, although this sophisticated attempt fails to interpret the magnetic properties such as the g^{eff}-values of Co(II)porphyrins.[6,7]

Lack of bridging the gap between the two cultures above has hampered more extensively embracing the concept of controllable spin–orbit couplings in chemistry and related fields. Attempting to bridge the gap, we have very recently derived exact or extremely accurate analytical expressions for the g^{eff}/g^{true} relationships for the spin quantum number S's up to S = 7/2.[11] The proposed method to directly convert the g^{eff}- to the g^{true}-values is facile generalization and affords relevant ZFS values, which gives a testing ground for both conventional and high-field/high-frequency (HF/HF) ESR analyses of high spin systems.

The proposed method has been underlain by exactly and analytically solving the eigenvalue/eigenfunction problems of a full spin Hamiltonian composed of the rank-2 ZFS tensor and electronic Zeeman interaction terms for a given spin quantum number up to S = 7/2, for the first time. The exact analytical formulas are given in terms of the principal-axis coordinate systems, and the method is free from the limitation to the magnitude of the microwave frequency and static magnetic field. Instead of performing advanced HF/HF ESR spectroscopy at cryogenic temperatures, we invoke both experiments and theoretical considerations to analyze the conventional X-band spectra from high spin metallocomplexes with sizable ZFS values. The complete spectral analyses are based on the exact diagonalization of the full spin Hamiltonians including ZFS and hyperfine tensors and on the exact analytical formulas for the canonical absorption peaks, which enable us to easily discriminate them from the off-principal axis extra peaks. The exact analytical expressions are based on the following spin Hamiltonian as given the rank-2 ZFS tensor and electron Zeeman interactions:

$$H = \boldsymbol{S}\cdot\mathbf{D}\cdot\boldsymbol{S} + \beta\boldsymbol{S}\cdot\mathbf{g}\cdot\boldsymbol{B} \quad (1a)$$

$$= D[S_z^2 - S(S+1)/3] + E(S_x^2 - S_y^2) + \beta(S_x g_x B_x + S_y g_y B_y + S_z g_z B_z) \quad (1b)$$

where equation (1b) is described in the principal coordinate axis system of the ZFS and **g**-tensors, which were assumed to be collinear in our previous work.[11] Note that we have removed the limitation of the collinearity in this work and generalized the proposed method, as described below. The generalization enables us to give relationships between relative orientations of the tensors, gaining important insights into the electronic structure of a high spin metal ion site. In this context, we have noted that any single-crystal ESR spectroscopy can afford key information on the relative orientations of the true **g**-tensors with respect to the principal axis coordinate system of the ZFS tensor, particularly.[11]

In the previous work, we have derived the extremely accurate analytical expressions of the g^{eff}/g^{true} relationships for high spin systems by using the genuine Zeeman perturbation approach, where the sizable ZFS terms **S** · **D** · **S** are fully diagonalized and electronic Zeeman terms are treated as perturbation to the desired order. The derived formula for the g^{eff}/g^{true} relationships are easy-to-access and the approach is advantageous to the exact analytical treatment in terms of mathematical complexity occurring with increasing the half-integer spin quantum number S (> 3/2). In the present generalization, we have taken advantage of the genuine Zeeman approach, showing a facile method to analyze fine-structure ESR spectra featuring in sizable ZFS tensors having no collinearity with **g**-tensors.

In this work, we have chosen, as three typical important examples so far documented, picket fence high spin porphyrins, [Mn^{II}(TpivPP)(1-MeIm)] (**1**, S = 5/2; TpivPP = α,α,α,α-tetrakis(*o*-pivalamidophenyl)-porphyrinato, 1-MeIm = 1-methylimidazole), [Mn^{II}(TpivPP)(2-MeHIm)] (**2**, S = 5/2; 2-MeHIm = 2-methylimidazole)[16] and [Fe^{III}(TMP)(4-ClPyNO)$_2$]BF_4 (**3**$^+$·BF_4^-, S = 5/2; TMP = tetramesitylporphyrin, 4-ClPyNO = 4-chloropyridine *N*-oxide)[17], and a pseudo-octahedral cobalt(II) complex, *cis*-[$Co(hfac)_2(H_2O)_2$] (**4**, S = 3/2; hfac = hexafluoroacetylacetonate).[18] They all are in the electronically high-spin ground states. The ESR spectra from the metalloporphyrins **1**–**3**$^+$ in their sextet state have been analyzed on the basis of the fictitious spin-1/2 approach.[16,17] We have

revisited them and carried out the complete analyses of their experimental ESR spectra and magnetic data in terms of the full spin Hamiltonian approach instead of the putative method, deriving their sizable ZFS parameters for the first time. The analyzed data can be compared with the corresponding theoretical values obtained by sophisticated quantum chemical calculations developed in our group.[19–25] The magnetic properties of the $Co^{II}(hfac)_2$ complex **4** in the spin-quartet ground state have been analyzed in terms of a Griffith spin Hamiltonian with ligand field parameters.[18] We have applied the currently developed generalized method to **4** and obtained somewhat different experimental data from the documentation, comparing them with our theoretical results. We emphasize that the present generalized analytical approach affords a clue to disclose the pitfalls associated with Co^{II} complexes in the quartet state, requiring more rectified theoretical considerations in terms of the construction of electron configurations for the ground state.

Direct conversion of the effective spin-1/2 g-values to the true g-values for the case of non-collinear g- and ZFS tensors: Comparison with the collinear cases for *S* = 3/2 and 5/2

The g^{eff}/g^{true} relationships require exact or extremely accurate expressions for resonance fields, and thus theoretically the eigenfield approach is the most suitable method which is capable of giving explicit formulas for the relationships if the linearization of the eigenfield solution is implemented.[26] Unfortunately, the mathematical complexity of the eigenfield solution hampers its application to the derivation of the relationships for high spin systems.[11] Alternatively, there are two approaches based on conventional eigenenergy solutions in the following: (1) Exact analytical approach and (2) genuine Zeeman perturbation treatment.[11] The exact energies in the principal axis coordinate system were analytically derived from the diagonalization of the rank-2 ZFS tensor + electronic Zeeman interaction spin Hamiltonian (Eq. 1). We have solved the corresponding higher-order algebraic equations, whose dimensions are reduced to be quadratic, cubic or quartic by using the conjugation symmetry of spinfunctions, giving the general solutions. In the genuine Zeeman perturbation treatment, the ZFS Hamiltonian is diagonalized in order to obtain the exact zeroth-order energies and wavefunctions, and the electronic Zeeman terms are treated as the perturbation to the second or third order. The g^{eff}/g^{true} relationships are obtained from Eq. (2) as a necessary condition, where $+M_S$ and $-M_S$ denote the conjugate spin sublevels:

$$E_{+Ms} - E_{-Ms} = g^{eff}\beta B \qquad (2)$$

where $E_{\pm Ms}$ is a function of only g^{true}, *D*, *E* and *B* in the case that the **g**- and ZFS tensors are assumed to be collinear.[11]

For the collinear cases:

For the spin-quartet state (*S* = 3/2), the g^{eff}/g^{true} relationships in the principal-axis system derived from the exact analytical diagonalization are[11,27,28]

$$\frac{g_x^{eff}}{g_x^{true}} = 1 \pm \frac{1-3\lambda}{\sqrt{1+3\lambda^2}} \qquad (3a)$$

$$\frac{g_y^{eff}}{g_y^{true}} = 1 \pm \frac{1+3\lambda}{\sqrt{1+3\lambda^2}} \qquad (3b)$$

$$\frac{g_z^{eff}}{g_z^{true}} = 1 \mp \frac{2}{\sqrt{1+3\lambda^2}} \qquad (3c)$$

where $\lambda = E/D$. The upper and lower signs correspond to $|M_S = \pm 1/2\rangle$ and $|M_S = \pm 3/2\rangle$ dominant transition, respectively. The g^{eff}/g^{true} relationships obtained from the genuine Zeeman perturbation treatment for the spin-quartet state are equivalent to the Eqs. (3a)–(3c) because of no energy corrections higher than the second order.

For the spin-sextet state (*S* = 5/2), the ZFS + Zeeman spin Hamiltonian in the case of ***B***//*z* is originally a 6 × 6 matrix and can be divided into two conjugate matrices whose basis sets are $\{|+5/2\rangle, |-3/2\rangle, |+1/2\rangle\}$ and $\{|-5/2\rangle, |+3/2\rangle, |-1/2\rangle\}$ due to the symmetry of the rank-2 ZFS tensor. The eigenvalues (E_n) and eigenfunctions of the former spin-conjugate set for the principal *z*-axis can be analytically obtained by the exact diagonalization in a trigonometric form;

$$E_n = 2a\cos\left(\frac{1}{3}\arccos\frac{b}{2a} + \frac{2n\pi}{3}\right) + \frac{1}{2}g_z^{true}\beta B$$

$$a = \frac{2}{3}\sqrt{7D^2 + 21E^2 + 6Dg_z^{true}\beta B + 3(g_z^{true}\beta B)^2}$$

$$b = \frac{40(D^3 - 9DE^2) + 36(4D^2 - 3E^2)g_z^{true}\beta B + D(g_z^{true}\beta B)^2}{21(D^2 + 3E^2) + 18Dg_z^{true}\beta B + 9(g_z^{true}\beta B)^2}$$

where *n* = 0, 1 and 2 correspond to $|M_S = +5/2\rangle$, $|M_S = -3/2\rangle$, and $|M_S = +1/2\rangle$ dominant magnetic sublevels, respectively. The exact energies for the $|M_S = -5/2\rangle$, $|M_S = +3/2\rangle$, and $|M_S = -1/2\rangle$ dominant states are obtained by replacing *B* to *–B* in the equations above. The corresponding g_z^{eff}/g_z^{true} relationships are obtained by Eq. (2). For the external magnetic field, ***B*** parallel to the principal *x*- or *y*-axis, the cyclic permutation for *D* and *E*, instead of formulating the original matrix for the principal *x*- or *y*-axis, gives the corresponding eigen-values/-functions and thus relationships of the replacement, i.e., $D \rightarrow (1/2)(3E - D)$ and $E \rightarrow (-1/2)(E + D)$ for ***B***//*x*, $D \rightarrow (-1/2)(3E + D)$ and $E \rightarrow (1/2)(E - D)$ for ***B***//*y* facilitate completing the derivations. All the expressions derived fulfil the global invariance above with respect to the cyclic permutation.[29–32]

The g^{eff}/g^{true} relationships in the principal-axis system for the spin-sextet state (*S* = 5/2) derived from the genuine Zeeman perturbation treatment are extremely accurate under the conditions of conventional ESR spectroscopy,[11] and they are mathematically simple as given in the following:

$$\frac{g_z^{eff}}{g_z^{true}} = \frac{\frac{50\lambda^2}{\left(x_n - \frac{10}{3}\right)^2} - \frac{54\lambda^2}{\left(x_n + \frac{2}{3}\right)^2} + 1}{\frac{10\lambda^2}{\left(x_n - \frac{10}{3}\right)^2} + \frac{18\lambda^2}{\left(x_n + \frac{2}{3}\right)^2} + 1} \qquad (4)$$

where $\lambda = E/D$ and x_n denotes the eigenenergy of the ZFS Hamiltonian in the units of *D*, explicitly given as follows.

$$x_n = 2a'\cos\left(\frac{1}{3}\arccos\frac{b'}{2a'} + \frac{2n\pi}{3}\right)/D$$

$$a' = \frac{2\sqrt{7}}{3}\sqrt{D^2 + 3E^2}$$
$$b' = \frac{40D(D+3E)(D-3E)}{21(D^2+3E^2)}$$

n = 0, 1 and 2 correspond to the $|M_S = \pm 5/2\rangle$, $|M_S = \pm 1/2\rangle$ and $|M_S = \pm 3/2\rangle$ dominant transition, respectively. The cyclic permutation of D and E shown above gives the g^{eff}/g^{true} relationships with $\boldsymbol{B}$ parallel to the principal x- and y-directions.[29–32] The global invariance holds in the genuine Zeeman perturbation treatment, as well. We have noted that for S = 5/2 the analytical expressions for the g^{eff}/g^{true} relationships based on the exact eigenenergy treatment are not practically nor mathematically simple, contrasting with those for S = 3/2. The genuine Zeeman perturbation treatment, however, gives both the mathematical simplicity and extreme accuracy for the spin-sextet and higher spin states, as shown above, affording physical insights into the relationships. The Zeeman perturbation treatment theoretically favors conventional X- or Q-band ESR spectroscopy over experimentally demanding HF/HF counterparts.[11]

For the non-collinear cases:

In some high spin metallocomplexes, the collinearity between their magnetic tensors does not a priori hold, and we have extended our previous approaches to such cases and derived the g^{eff}/g^{true} relationships by relaxing the assumption of the collinearity between **g**- and **D**-tensors. We have noted that the general but facile and simple formulas are not expected to come out, but the derived expressions serve to check the influence caused by the definitions for the principal effective spin 1/2 g-values and spurious arguments for powder-pattern ESR spectral analyses of such non-collinear cases. From the experimental side, an elaborate single crystal experiment plays an essential role for the occurrence of the non-collinearity.[11] From the theoretical side, the occurrence of the non-collinearity gives a testing ground for the improvement of theory. Additionally, reliable quantum chemical calculations make significantly meaningful predictions for the non-collinearity. In contrast to the simple expressions Eqs. (3a)–(3c) derived under the assumption of the collinearity, the non-collinearity lowers the symmetry of the spin Hamiltonian and thus the spin-conjugate approach cannot be applicable because the non-collinearity gives rise to the appearance of additional off-diagonal elements such as $S_x g_{xz'} \beta B$ and $S_y g_{yz'} \beta B$ which break the spin-conjugate relationship, as shown below. Non-collinearity makes the expressions for the g^{eff}/g^{true} relationships with S = 3/2 more complex, but affords the possible determination of sizable ZFS tensors in some favorable cases of powder-pattern ESR spectroscopy, as shown later and ESI.

The principal axis coordinate system (x, y, z) is taken as that of the rank-2 ZFS tensor. Introducing the direction cosines, cos $\vartheta_{ij'}$'s, which define the relative orientation of the non-collinear **g**-tensor with respect to the ZFS **D**-tensor. $\vartheta_{ij'}$ (i = x, y, z; j' = x', y', z') is an angle between the i-axis of the **D**-tensor and the j'-axis of the **g**'-tensor. Thus, a transformation matrix U is given as

$$U = \begin{pmatrix} \cos\theta_{xx'} & \cos\theta_{xy'} & \cos\theta_{xz'} \\ \cos\theta_{yx'} & \cos\theta_{yy'} & \cos\theta_{yz'} \\ \cos\theta_{zx'} & \cos\theta_{zy'} & \cos\theta_{zz'} \end{pmatrix}$$

The **g**'-tensor is given in its original principal coordinate axis system (x', y', z') as

$$\mathbf{g}' = \begin{pmatrix} g_{x'} & 0 & 0 \\ 0 & g_{y'} & 0 \\ 0 & 0 & g_{z'} \end{pmatrix}$$

The matrix U transforms **g'** into **g** in terms of the principal coordinate axis system (x, y, z) as

$$\mathbf{g} = U\mathbf{g}'U^{\mathrm{T}} = \begin{pmatrix} \cos\theta_{xx'} & \cos\theta_{xy'} & \cos\theta_{xz'} \\ \cos\theta_{yx'} & \cos\theta_{yy'} & \cos\theta_{yz'} \\ \cos\theta_{zx'} & \cos\theta_{zy'} & \cos\theta_{zz'} \end{pmatrix} \begin{pmatrix} g_{x'} & 0 & 0 \\ 0 & g_{y'} & 0 \\ 0 & 0 & g_{z'} \end{pmatrix} \times \begin{pmatrix} \cos\theta_{xx'} & \cos\theta_{yx'} & \cos\theta_{zx'} \\ \cos\theta_{xy'} & \cos\theta_{yy'} & \cos\theta_{zy'} \\ \cos\theta_{xz'} & \cos\theta_{yz'} & \cos\theta_{zz'} \end{pmatrix}$$

where U^{T} denotes the transposed matrix of U. The rank-2 ZFS and electronic Zeeman interaction Hamiltonian is given in the principal axis coordinate system as Eq. (1a). When the static magnetic field is oriented along the z-axis, i.e., with $\boldsymbol{B} = (0, 0, B)^{\mathrm{T}}$, H is given as

$$H = D\left[S_z^2 - \frac{1}{3}S(S+1)\right] + E\left(S_x^2 - S_y^2\right) + \left(S_x g_{xz'} + S_y g_{yz'} + S_z g_{zz'}\right)\beta B$$

where $g_{ij'}$ denotes the ij' component of the **g**-tensor in terms of the principal axis coordinate system (x, y, z), i.e., the one for the ZFS tensor, defined as

$$g_{xz'} = g'_{xz} = g_{x'}\cos\theta_{xx'}\cos\theta_{zx'} + g_{y'}\cos\theta_{xy'}\cos\theta_{zy'} + g_{z'}\cos\theta_{xz'}\cos\theta_{zz'},$$

$$g_{yz'} = g'_{yz} = g_{x'}\cos\theta_{yx'}\cos\theta_{zx'} + g_{y'}\cos\theta_{yy'}\cos\theta_{zy'} + g_{z'}\cos\theta_{yz'}\cos\theta_{zz'},$$

$$g_{zz'} = g'_{zz} = g_{x'}\cos^2\theta_{zx'} + g_{y'}\cos^2\theta_{zy'} + g_{z'}\cos^2\theta_{zz'},$$

Since there is no confusion as to the definition of the principal axis coordinates, we introduce g'_{ij} instead of $g_{ij'}$ for simplicity. Throughout the derivation below, the prime of g'_{ij} is kept so as to represent the non-collinearity of the **g**-tensor.

The matrix representation of the rank-2 ZFS tensor + electronic Zeeman interaction Hamiltonian in the case of the spin quartet state is given in the $|M_S\rangle$ basis set as

$$\begin{pmatrix} D + \frac{3}{2}g'_{zz}\beta B & \frac{\sqrt{3}}{2}(g'_{xz} - ig'_{yz})\beta B & \sqrt{3}E & 0 \\ \frac{\sqrt{3}}{2}(g'_{xz} + ig'_{yz})\beta B & -D + \frac{1}{2}g'_{zz}\beta B & (g'_{xz} - ig'_{yz})\beta B & \sqrt{3}E \\ \sqrt{3}E & (g'_{xz} + ig'_{yz})\beta B & -D - \frac{1}{2}g'_{zz}\beta B & \frac{\sqrt{3}}{2}(g'_{xz} - ig'_{yz})\beta B \\ 0 & \sqrt{3}E & \frac{\sqrt{3}}{2}(g'_{xz} + ig'_{yz})\beta B & D - \frac{3}{2}g'_{zz}\beta B \end{pmatrix}$$

Note that the symmetry of the conjugate spin eigenfunctions is broken because of the non-collinearity of the **g**-tensor in contrast to the collinear case. The exact eigenenergies E can be analytically solved as follows:

$$E = \frac{1}{2}\left[\pm_1\sqrt{u_0}\pm_2\sqrt{-2q - u_0 \mp_1 \frac{2p}{\sqrt{u_0}}}\right]$$

$$u_0 = 2a_0\cos\left(\frac{1}{3}\arccos\frac{b_0}{2a_0}\right) - \frac{2q}{3}$$

$$a_0 = \frac{1}{3}\sqrt{p^2 + 12r}$$

$$b_0 = \frac{2p^3 - 27q^2 + 72pr}{3p^2 + 36r}$$

$$p = -2D^2 - 6E^2 - \frac{5}{2}\left(g'_{zz}\beta B\right)^2 - \frac{5}{2}\left(g'_{xz}{}^2 + g'_{yz}{}^2\right)(\beta B)^2$$

$$q = -4D\left(g'_{zz}\beta B\right)^2 + 2D\left(g'_{xz}{}^2 + g'_{yz}{}^2\right)(\beta B)^2 - 6E\left(g'_{xz}{}^2 + g'_{yz}{}^2\right)(\beta B)^2$$

$$\begin{aligned} r = {} & (D^2 + 3E^2)^2 - \frac{5}{2}D^2\left(g'_{zz}\beta B\right)^2 + \frac{9}{2}E^2\left(g'_{zz}\beta B\right)^2 \\ & + \frac{1}{4}D^2\left(g'_{xz}{}^2 + g'_{yz}{}^2\right)(\beta B)^2 \\ & + 6DE\left(g'_{xz}{}^2 + g'_{yz}{}^2\right)(\beta B)^2 \\ & - \frac{9}{2}E^2\left(g'_{xz}{}^2 + g'_{yz}{}^2\right)(\beta B)^2 + \frac{9}{8}\left(g'_{zz}\beta B\right)^4 \\ & + \frac{9}{16}\left(g'_{zz}\beta B\right)^2\left(g'_{xz}{}^2 + g'_{yz}{}^2\right)(\beta B)^2 \\ & + \frac{9}{16}\left(g'_{xz}{}^2 + g'_{yz}{}^2\right)^4(\beta B)^4 \end{aligned}$$

The corresponding eigenfunctions can also be derived analytically. Thus, the any transition probabilities can be obtained. The relationships between the g^{eff}- and g^{true}-values for the transition relevant to the $|M_S\rangle$ dominant Kramers doublets become complex as expected for the non-collinearity effect due to the contributions from the other principal g-values such as $g_{x'}$ and $g_{y'}$. Thus, we solve the simultaneous equations associated with the relationships from the other principal orientations in order to get the expressions between the $\mathbf{g}^{\text{eff}}$- and $\mathbf{g}^{\text{true}}$-tensors. It should be noted that the genuine Zeeman perturbation formalism below can afford more facile generalization, as described in the previous paper,[11] and useful approach to gain physical insights into the effects caused by the non-collinearity and the symmetry reduction of the conjugate spinfunctions caused by the additional Zeeman interaction terms.

For the other principal axis orientations such as for ***B***//x, as well known, the cyclic permutation of the subscripts for the axes, $D_z \rightarrow D_x$, $D_x \rightarrow D_y$, $D_y \rightarrow D_z$, gives the eigenvalues and functions relevant to the ZFS **D**-tensor, as the transformation procedure explicitly described above for the collinear case.[29–32] The transformation associated with the **D**-tensor described in terms of the principal axis coordinate system is straightforward because there is no off-diagonal element of the tensor.

For the case of the non-collinearity, the equations above include the off-diagonal elements of the **g**-tensors, and the effects of any change in the principal axis coordinate system on the transformation between two tensors, T and T' should be mentioned. The effects are described in terms of the general properties of the transformation, in which the direction cosines (a_{ik}'s) defining the relative orientation between the axes of the two tensors. The transformation associated with the present cyclic permutation with respect to the three orthogonal coordinate axes involves only three non-vanishing a_{ik}'s (= 1) for one cyclic permutation, proving that all the diagonal and off-diagonal elements can be transformed into the elements governed by the transformation rule, $T_{ij'} = \Sigma\, a_{ik}\, a_{jl}\, T_{kl}$ (k, l = 1, 2, 3). Thus, for the other principal axis orientations the transformation relevant to the **g**-tensor can be carried out by the cyclic permutation of the subscripts for the x, y and z axis, i.e., for ***B***//x the facile transformation, $z \rightarrow x$, $x \rightarrow y$, $y \rightarrow z$ affords the corresponding eigenvalues/eigenfunctions in a straightforward manner. The global invariance of the $g^{\text{eff}}/g^{\text{true}}$ relationships with respect to the axis transformations holds for the non-collinear case. This is also true for the formulas derived on the genuine Zeeman perturbation treatment for the non-collinearity, described in ESI.

We note that the current exact analytical method is hampered by the lack of algebraic analytical expressions for the general solutions of quintic and higher than fifth order algebraic equations, although there are non-algebraic general solutions for quintic equations[33] and what is worse for the non-collinear cases the exploitation of the symmetry of spin conjugate eigenfunctions for higher spin quantum number S's is not applicable. Thus, the capability of the method is limited, but we emphasize that the Zeeman perturbation treatment, which gives extreme accuracy for conventional X- or Q-band ESR spectroscopy, is free from such limitation for the higher S's. The genuine Zeeman perturbation treatment with the aid of hypergeometric functions[33] allows us to derive analytical expressions for the $g^{\text{eff}}/g^{\text{true}}$ relationships for the spin quantum number S's up to S = 9/2 without collinearity.

To illustrate the usefulness of the present method for the non-collinearity, we have carried out model calculations of the relationships between $\mathbf{g}^{\text{eff}}$- and $\mathbf{g}^{\text{true}}$-tensors, in which the magnetic tensors of *cis*-[Co(hfac)$_2$(H$_2$O)$_2$] (**4**) are taken. In the model calculations, the principal coordinate axes of the **g**-tensor are rotated around one principal axis of the **D**-tensor. Explicit appearance of the effects of the non-collinearity on the ESR fine-/hyperfine structure spectra is displayed in details (see ESI: Fig. S1).

The simulated ESR spectra and energy-level diagrams presented in this work were calculated by using of EasySpin (ver. 5.1.12).[34] The magnetic susceptibility measurements of **3** and **4** were simulated by using of the curry function of EasySpin (ver. 5.1.12) and a laboratory-built program on MATLAB 2014B.[11] All the details of the analyses of the magnetic data are given in ESI.

Quantum Chemical Calculations

Quantum chemical calculations were carried out in order to estimate the theoretical magnetic tensors of the sextet (Mn(II) complexes **1**, **2** and Fe(III) complex, $\mathbf{3}^{+}$) and quartet (cobalt(II) complex, **4**) ground states, comparing them with the experimental true **g**- and ZFS tensors, as determined in this

work for the first time. Their single point calculations were carried out by using the solid state geometries reported from the X-ray crystallography.[16–18] The electronic configuration of the Mn(II) and Fe(III) center is d^5 in the high spin state and therefore all valence d orbitals are singly occupied. Such an electronic configuration can be safely described within the framework of single-reference theory. Thus, we adopted DFT-based approaches for the magnetic tensor calculations of the Mn(II) complexes **1** and **2**, and Fe(III) complex $\mathbf{3}^+$. The **g**-, **A**- and $\mathbf{D}^{SS}$-tensors of the Mn(II) complexes **1** and **2**, and Fe(III) complex $\mathbf{3}^+$ were calculated at the UBP86/Sapporo-DZP by using of ORCA (ver. 3.0.0) software,[35] and the $\mathbf{D}^{SO}$-tensor calculations were performed at the natural orbital-based Pederson–Khanna (NOB-PK)[24] method with the GAMESS-US program[36] and our-own codes. $\mathbf{D}^{SS}$ and $\mathbf{D}^{SO}$ denote the contribution of the ZFS (**D**) tensor from the spin-spin coupling and the spin–orbit interaction, respectively. Note that in the DFT-based framework spin–orbit Hamiltonian with effective nuclear charges was adopted and therefore two-electron spin-same-orbit and spin-other-orbit terms were not included, because only one-electron density matrices are available in DFT. The NOB-PK method can predict $\mathbf{D}^{SO}$-tensors of the transition metal complexes more accurately than the conventional approaches like Pederson–Khanna (PK) and coupled-perturbed (CP) methods, if the static Jahn–Teller distortion is not present.[24,25] In the NOB-PK calculations the BP86 exchange–correlation functional was adopted and the Sapporo-DZP and 3-21G basis sets were employed for metal centers and other atoms, respectively.

The d-electron configuration of the Co(II) complex **4** is d^7 and therefore the two of the quasi-degenerate t_{2g} orbitals are doubly occupied and one of them is singly occupied in the electronic ground state, and static Jahn–Teller distortion is present. We emphasize that in this electron configuration the ground state wavefunction is expected to have a strong multi-configuration character, and many excited states are located close to the ground state. DFT-based approaches are inadequate for the magnetic tensor calculations of such systems and therefore we adopted the complete active space self-consistent field (CASSCF)-based approaches. The **g**-tensor of the Co(II) complex **4** was calculated using the sum-over-states (SOS) equation in conjunction with the state-specific CASSCF(7e,5o) wavefunction, and the $\mathbf{D}^{SO}$-tensor was computed with the help of the hybrid CASSCF/multireference second-order Møller–Plesset perturbation theory (MRMP2) method, as proposed by us.[20] The def2-TZVP and def2-SVP basis sets were employed for Co(II) and other atoms, respectively. In the MRMP2 calculations, the energy denominator shift technique[37] was adopted for the intruder state avoidance, with the shift parameter $\Delta = 0.02$ Hartree. The **g**- and $\mathbf{D}^{SO}$-tensor calculations were performed by using ORCA and GAMESS-US programs, respectively.

Results and discussion

(a) [Mn^{II}(TpivPP)X] (1, X = 1-MeIm; 2, X = 2-MeHIm; $S = 5/2$): Picket fence high spin metalloporphyrin in the ground state

Porphyrin chemistry underlain by biological implications has been expanded, and vast numbers of metalloporphyrin complexes have been synthesized, imitating reactions in biological systems, and the electronic structures of their open shell counterparts have extensively been discussed in terms of electron magnetic spectroscopy including Electron-Nuclear DOuble Resonance (ENDOR).[1,38–42] Importantly, picket fence porphyrins were reported by Collman and co-workers in 1975 as model compounds of hemoproteins with oxygen binding in the biological systems.[43,44] High spin manganese(II) porphyrin complexes have isoelectronic structures of high spin iron(III) complexes, but give somewhat different spin parameters, particularly their *D*-values.[45] Yu and co-workers reported the ESR spectra of 5-coordinated Mn(II) porphyrin complexes in their spin-sextet ground state.[16] The conventional X-band ESR spectrum of the powdered sample of complex **1** reveals at maximum five distinguishable resonance peaks whose *g*-values in terms of the fictitious spin-1/2 Hamiltonian approach range in magnitude from 0.5 to 6. Such a wide range of the effective *g*-values is indicative of the occurrence of the spin-sextet state if they all are attributable to the same origin, but the spectral analysis based on the fictitious spin-1/2 spin Hamiltonian approach is hampered by a lack of any significant modification by the ZFS tensor although the approach affords the assignment of off-principal axis extra peaks due to large anisotropy of both the hyperfine coupling and **g**-tensors. Very few papers can be found on the full analysis (fictitious spin-1/2 spin Hamiltonian approach) including the off-axis extra lines of ESR spectra of Mn(II) complexes having the ZFS parameters comparable to the energy of the irradiating microwave (e.g., about 0.3 cm^{-1} for X-band).[46] We point out that the angular dependence of the fine-/hyperfine structure ESR spectra with respect to the static magnetic field often features in discontinuous-looping transitions in the range of off-principal axis directions of the magnetic field as typically shown in Fig. 1b, whose stationary points with respect to the orientation angles give the off-axis peaks.[11,26,47–49] The complete assignment of the off-axis extra peaks together with the principal canonical peaks in the powder-pattern spectra can afford quantitative information on both the ZFS and true **g**-tensors, which are to be compared with reliable quantum chemical calculations. As the important model metalloporphyrins, we have revisited the documented randomly-oriented ESR spectra of the two complexes, [Mn^{II}(TpivPP)X] (**1**, X = 1-MeIm; **2**, 2-MeHIm), whose porphyrin scaffold is planar, by invoking the full spin Hamiltonian (the rank-2 ZFS tensor + electronic Zeeman interaction Hamiltonian) (Eq. 1) with the proposed method for the g^{eff}/g^{true} relationships,[11] showing an intrinsic advantage over the putative effective (fictitious) spin-1/2 Hamiltonian approach.

The principal values of the **g**-tensor for the complex **1** and **2**, as revisited and reanalyzed in terms of the full spin Hamiltonian approach, are close to 2.0023, the *g*-factor of the free electron. The magnitude of their *D* values is about 20 GHz (0.67 cm^{-1}) and $E/D \leqq 0.005$ (see the caption of Fig. 1 and Table S2 for detail). During the analyses, the microwave frequency available was only of three significant figures such as 9.45 GHz given in Fig. 1. Figure 1 shows only the simulated ESR spectrum (Fig. 1a) for the

frozen solution sample of **2** observed at 90 K and the whole angular dependence (Fig. 1b and 1c) of the ESR transitions (resonance fields and their transition intensities depicted) by using both the fictitious spin-1/2 Hamiltonian (the spectrum in blue) and the full spin Hamiltonian (the spectrum in red). The magnetic tensors are assumed to be collinear, and the angular dependence in the full spin Hamiltonian approach is given in the principal axis coordinate systems. Many off-principal axis extra transitions are expected to appear and identified, which reproduced the experimentally observed but unidentified peaks in the document. As clearly seen in Fig. 1, significant contribution from the presence of the ZFS tensor is apparent for the off-axis extra peaks such as subtle spread of the lineshapes (the red spectrum in Fig. 1a), while the fictitious spin-1/2 Hamiltonian method cannot afford any important information on the off-axis extra peaks, as seen in the blue spectrum Fig. 1a. We have noticed that such spread shows up in the documented experimental spectra as 5–15 times magnified.[16] In this context, we emphasize that the off-principal axis extra peaks do not appear in the spectral simulation based on the fictitious spin-1/2 Hamiltonian for complex **2**, which never reproduces the resonance fields and lineshapes of the experimental ones documented,[16] illustrating a serious breakdown of the putative fictitious spin-1/2 Hamiltonian approach. We have also noticed that the experimental principal values of the hyperfine coupling tensors of the Mn(II) atom significantly differ between the two approaches, reflecting the difference in the hyperfine projection factor 2*S* relevant to the spin multiplicity.[11]

Quantum chemical calculations of the hyperfine coupling tensors should be relevant to the true hyperfine principal values obtainable in terms of the full spin Hamiltonian approach. They give a testing ground for reliability of the calculations, as discussed below. Significantly, the *E*/*D* ratio of **1** is smaller than that of **2**, reflecting the higher symmetry of the porphyrin skeleton in which the bond lengths between the manganese and the pyrrole nitrogen atoms are almost the same, revealing an increase in the axial symmetry.

In the full spin Hamiltonian approach, the "g^{eff} = 6 and 2" lines are due to the typical $|M_S = \pm 1/2\rangle$ dominant transitions for the principal *x*- and *y*-axes and *z*-axis, respectively.[11,46] The additional peaks at about 600 mT, 870 mT and 1250 mT are assigned to the off-principal axis extra lines as identified in Fig. 1b. A part of the peak with g^{eff} = 1.23 is attributable to the $|M_S = \pm 3/2\rangle$ dominant transition in the canonical *x*- and *y*-axes (see Table. S1 for details). The calculated transition probabilities indicate the hyperfine forbidden transitions enhanced by the parallel excitation along the static magnetic field. Importantly, in the analysis revisited, the best fit spin Hamiltonian parameters of complex **1** and **2**, except for electric quadrupolar coupling constants of the Mn(II) atom, in terms of both the fictitious spin-1/2 and full spin Hamiltonian approaches are determined, and the true principal *g*-values and other spin Hamiltonian parameters are accurate enough to compare with reliable quantum chemical calculations. The magnetic tensors are assumed to be collinear in the analyses.

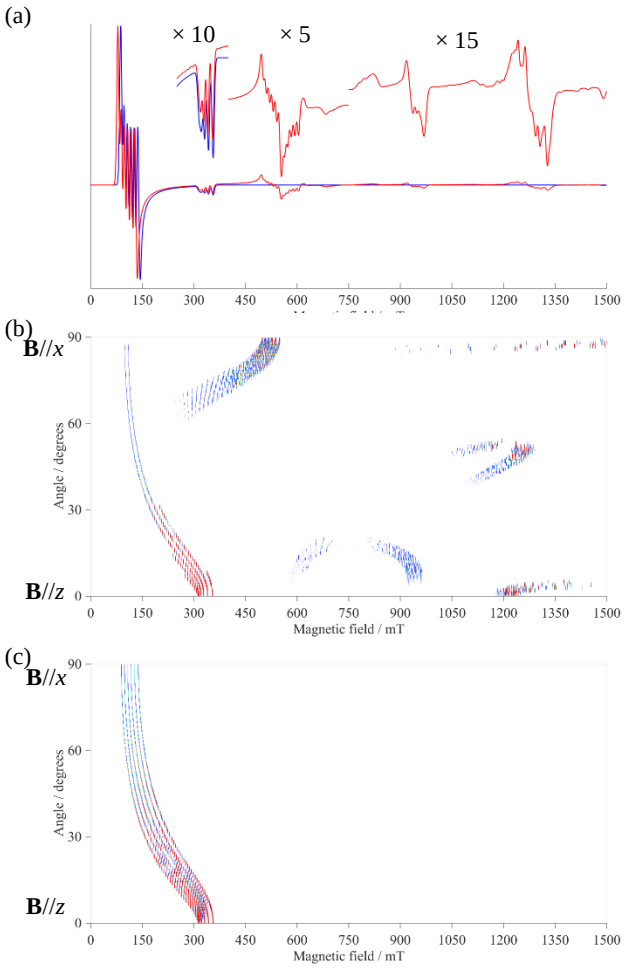

Fig. 1. Simulated X-band (9.45 GHz) ESR spectra of the rigid-glass sample of the Mn(II) complex **2**, based on both the fictitious spin-1/2 (blue) Hamiltonian and full spin Hamiltonian approach (red). The experimentally determined spin Hamiltonian parameters are as follows: The blue ESR spectrum in Fig. 1a is simulated by a set of the parameters, $g_{1,x}^{\mathrm{eff}}$ = 5.9, $g_{1,y}^{\mathrm{eff}}$ = 5.9, $g_{1,z}^{\mathrm{eff}}$ = 1.96, $A_{1,x}^{\mathrm{eff}}(^{55}\mathrm{Mn})$ = 750 MHz, $A_{1,y}^{\mathrm{eff}}(^{55}\mathrm{Mn})$ = 750 MHz, $A_{1,z}^{\mathrm{eff}}(^{55}\mathrm{Mn})$ = 240 MHz with the peak-to-peak linewidth of 7 mT. The red ESR spectrum in Fig. 1a is simulated by a set of the parameters, S = 5/2, g_x = 2.19, g_y = 2.12, g_z = 1.96, $A_x(^{55}\mathrm{Mn})$ = 280 MHz, $A_y(^{55}\mathrm{Mn})$ = 270 MHz, $A_z(^{55}\mathrm{Mn})$ = 240 MHz, D = 0.7 cm^{-1}, E/D = 0.004 with the peak-to-peak linewidth of 7 mT. Any strain effect on the linewidth is not included. The angular dependence of the ESR spectra from the principal *z*- to *x*-axis are shown for simplicity: Fig. 1b and c for the full spin Hamiltonian and fictitious spin-1/2 Hamiltonian approach, respectively. The complete angular dependence including all the transitions to construct the powder-pattern spectra is given in ESI (Figs. S3 and S5). The simulated spectra were obtained using EasySpin (ver. 5.1.12)[34] with varying the orientation of the magnetic field one-degree stepwise. Quadrupolar interaction terms of ^{55}Mn(II) were not explicitly included in the spectral simulation. Colors denote the transition intensities; typically blue denotes the low intensity and red the high intensity.

The DFT-based quantum chemical calculations were carried out in order to obtain the theoretical spin Hamiltonian parameters of complex **1** and **2**. The calculated parameters are summarized in Table S3. The calculated *D*-values (*D* = +0.5578 and +0.4933 cm^{-1} for **1** and **2**, respectively by NOB-PK[24]) are positive for both the complexes. The calculations seem to well reproduce the experimental values, while the PK method does not. The calculated *D*-values are 20–30% underestimated while the *E*-values are overestimated for both the complexes with respect to the experimental results. The overestimated ratios of $|E/D|$ originate in the departure from the axial symmetry of the

theoretical magnetic tensors, being indicative of requiring more rectified theoretical considerations. Figure 2 shows the calculated spin density distributions and principal axes of **D**-, **g**- and **A**(^{55}Mn)-tensors of complex **1** and **2**. They are collinear and reasonably the principal *z*-axis is perpendicular to the porphyrin plane and the *x* and *y*-axes lie in the porphyrin plane. We emphasize that the theoretical principal *g*-values for both the complexes satisfactorily agree with the experimentally determined true *g*-values. The significantly less anisotropic nature of the true **g**-tensors reflects the electron configuration of the Mn(II) atom. It is significant to note that the spin-sextet Mn(II) planar porphyrins without the 6th ligand coordination feature in the order of +0.5 cm^{-1} for the *D*-value, while spin-sextet Fe(III) porphyrins in one order of the magnitude large *D*-values.[11]

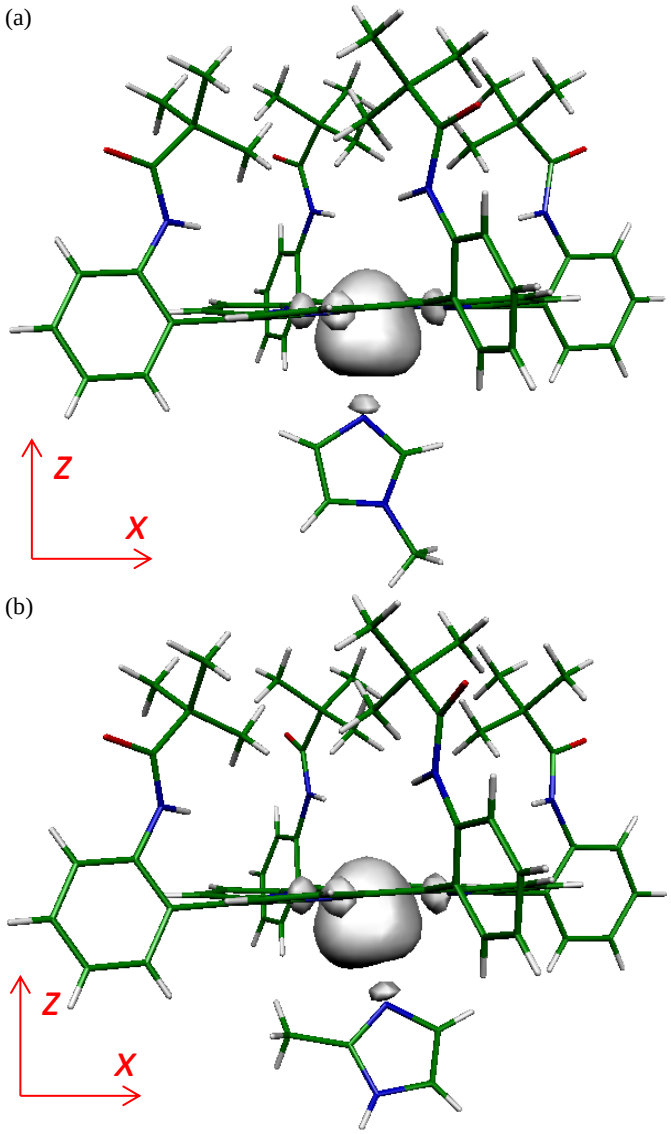

Fig. 2. The calculated spin density distributions and principal axes of **D**-, **g**- and **A**(^{55}Mn)-tensors of (a) the Mn(II) complex **1** and (b) the complex **2**. The principal *z*-axis is perpendicular to the Mn-N bonds and the *x*- and *y*-axes lie in the porphyrin plane.

(b) [Fe(TMP)(4-ClPyNO)$_2$]BF$_4$ (3$^+$·BF$_4^-$, *S* = 5/2): A spin-sextet ferric ion porphyrin in the ground state with the 6th coordination

Ferric iron porphyrin complexes are found in hemoglobin and myoglobin, and they are extensively distributed among biological systems as iron carriers such as transferrins.[1–3,40,42,50] Iron(III) (3d^5) ion can take three spin states, *S* = 1/2, 3/2 and 5/2 which are changeable with and without the 5th and 6th coordination ligands, for example, oxygen molecule and/or the side chains of amino acids. Spin crossover phenomena between the spin states are phenomenologically triggered by various stimuli such as temperature, pressure, light and so on. Recently, Ide and co-workers have reported [Fe(TMP)(4-ClPyNO)$_2$]BF$_4$ (**3**$^+$·BF$_4^-$) as the 6-coordination complex with a spin-sextet (*S* = 5/2) ground state, which exhibits the spin crossover phenomena between the high spin and low spin (*S* = 1/2) states.[17] The X-band ESR spectrum of the high spin complex **3**$^+$·BF$_4^-$ showed the "g^{eff} = 6 and 2" lines in terms of the fictitious spin-1/2 Hamiltonian approach, which are typical of the ferric ion complex in the sextet ground state with a sizable *D*-value. We have revisited complex **3**$^+$·BF$_4^-$ and carried out to estimate the principal values of the true magnetic tensors with the help of the full spin Hamiltonian composed of the rank-2 ZFS tensor + electronic Zeeman interaction Hamiltonian. We focus on the magnitude of the ZFS parameter, *D*-value for the ferric iron porphyrin with the planar porphyrin skeleton of complex **3**$^+$.

We first describe the computational results for complex **3**$^+$. There exist two molecules of complex **3**$^+$ in a unit cell with the different energies and Fe-O bond length: 2.054 Å/2.055 Å for the lower and 2.038 Å for the higher. The calculations were carried out for the molecule with the lower energy. Figure 3 shows the calculated spin density distribution and the computational axes of **3**$^+$, which correspond to the principal-axis systems of the magnetic tensors. A counter anion (BF$_4^-$) was not included in the calculations, not giving significant influence on the evaluation of the tensors. The calculated *D*- and *E*-values are +3.1241 cm^{-1} and –0.0830 cm^{-1}, as acquired by the improved NOB-PK method (Table S4), indicating that significant departure from the axial symmetry of the theoretical ZFS tensor is expected. We note, however, that this sizable degree of the asymmetry contradicts the experimental observation, whereas the order of the magnitude for the *D*-value and its sign seems reasonable, considering the accuracy of the theoretical method for the 3d^5 electron configuration of ferric iron cases.[11,51] As described above in (a) for the case of the Mn(II) porphyrins, the theory still overestimates the degree of the asymmetry. Importantly, the theoretical *D*-value of complex **3**$^+$, +3.1241 cm^{-1} can be compared with the experimental one, which falls in the range of order of cm^{-1} to 10 cm^{-1}, as determined by the magnetic susceptibility analysis revisited in this work (see below and Fig. S9). Referred to the theoretical principal *g*-values, they all are very close to 2.00, agreeing with the experimental true principal *g*-values, as given in Table 1, obtained in terms of the full spin Hamiltonian approach.

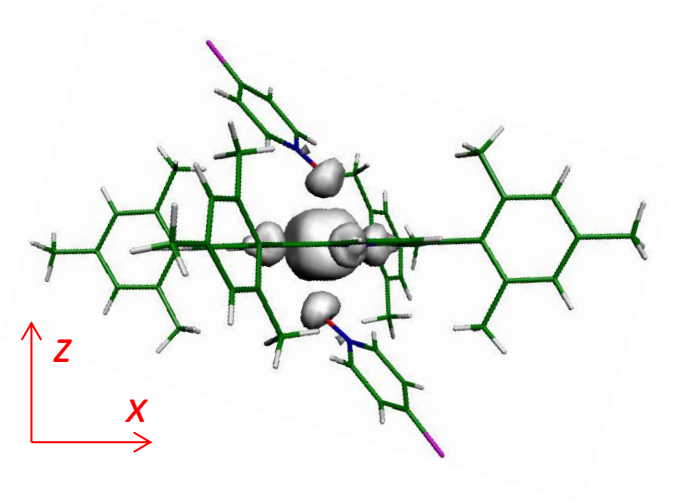

Fig. 3. The calculated spin density distributions and the computational axes of the ferric iron complex $\mathbf{3}^{+}$. The principal *z*-axis is perpendicular to the porphyrin plane and the principal *x*- and *y*- axes lie in the porphyrin plane.

Sizable *D*- and *E*-values of high spin metalocomplexes can be estimated from the temperature dependence of the effective magnetic moment (μ_{eff}) from the experimental side. Since no information on the ZFS parameters of complex $\mathbf{3}^{+}$ has been documented, we have revisited the magnetic susceptibility analysis of complex $\mathbf{3}^{+}$.[17] Although not given the detailed data enough to complete the analysis, we have noticed that the calculated μ_{eff}/μ_B values of complex $\mathbf{3}^{+}$ as simulated by using the spin-sextet full spin Hamiltonian exceeded the experimental ones even at the limit of $E/D = 0$ (Fig. S9). On the other hand, the fine-structure ESR spectra documented explicitly show that they are attributable to the case close to the limit, contradicting our analysis of the SQUID measurements on complex $\mathbf{3}^{+}\cdot BF_4^{-}$. Indeed, our present magnetic susceptibility analysis excludes any possible contribution from nearby electronic excited states of complex $\mathbf{3}^{+}$, consulting simple quantum chemical considerations, but this may not be the case. We have also excluded any possible contribution from complex $\mathbf{3}^{+}$ having the different Fe-O bond length and energy in the present analysis. In order to extract the ZFS parameters from the SQUID data documented, we have safely assumed that the $|E/D|$ value is small, as suggested by the observed ESR spectra and the magnetic tensors are collinear. We have derived positive *D*-values smaller than 10 cm^{-1} from the μ_{eff}/μ_B curve fitting with a set of the fixed principal values for the true **g**-tensors, which were directly obtained from the g^{eff}/g^{true} relationships based on the genuine Zeeman perturbation treatment (eq. 4). In the fitting procedure, we have elaborately analyzed the initial rise of the μ_{eff}/μ_B curve appearing at low temperature.[17] We point out that the *D*-value extracted above is reduced of any possible experimental or theoretical corrections are made on the SQUID data. In Table 1, the principal values of the magnetic tensors for the Fe(III) complex $\mathbf{3}^{+}\cdot BF_4^{-}$ are given together with the ratios of g^{eff}/g^{true}. The simulated X-band ESR spectra using the experimentally determined spin Hamiltonian parameters are shown in Fig. S10.

Table 1. The principal values of the magnetic tensors of $\mathbf{3}^{+}\cdot BF_4^{-}$. The columns denoted by "true" and "effective" give the values based on the ZFS + electronic Zeeman interaction Hamiltonian and the fictitious spin-1/2 Hamiltonian approaches, respectively.

	true	effective	g^{eff}/g^{true}
g_x	1.996	5.94	2.976
g_y	1.965	5.94	3.023
g_z	1.99	1.99	1.00
D/cm^{-1} (> 0)	< 10.0*	Not available	
E/D	< 0.001	Not available	

* The value was obtained from the analysis of the magnetic susceptibility data documented[17] by invoking the full spin Hamiltonian approach combined with the g^{eff}/g^{true} relationships.

The angular dependence of the simulated X-band ESR spectra suggests that the other transitions could be observed at about 2900 mT and 3200 mT for the principal *x*- and *y*-axis, respectively (Fig. S12). These transitions are assigned to the $|M_S = \pm 3/2\rangle$-dominant transition (Fig. S12). When the single-crystal ESR measurement available, the additional signal could be obtained at some angle.

(c) *cis*-[Co(hfac)$_2$(H$_2$O)$_2$] (4, *S* = 3/2)

Spin-quartet cobalt(II) complexes in the ground state possess sizable ZFS parameters with the implication of new molecular functionality such as single-molecule magnets (SMMs), which are underlain by the possible high energy barrier of the spin flip and the long relaxation time.[18,52] Recently, hexa-coordinated (pseudo-octahedral) high spin cobalt(II) complexes with sizable ZFS parameters comparable to the microwave excitation energy of X-band ESR (9.5 GHz or 0.3 cm^{-1}) have been studied.[18,28,51–64] Palii and co-workers synthesized $NH_4[Co^{II}(hfac)_3]$ and investigated the electronic structures and magnetic characters as SMM by using of ESR spectroscopy and AC/DC magnetic susceptibility measurements.[51] From the theoretical viewpoint, the principal values of the magnetic tensors such as the **g**-, ZFS **D**- and hyperfine **A**-tensors for the $3d^7$ electron configuration of high spin metal ions are still the focus of the current quantum chemical calculations.[61,63] Identification of the principal axes of the ZFS tensor with respect to the **g**-tensor or molecular frame is of crucial importance, giving a testing ground for theory.[11] In this context, single-crystal ESR spectroscopy gives a key to check the reliability of both the method for spectral analyses and the theoretical considerations, although there have not been many single-crystal ESR studies for Co(II) complexes in the high-spin ground state.

A Co(II) complex, *cis*-[Co(hfac)$_2$(H$_2$O)$_2$] (**4**), which has recently been reported by Korchagin and co-workers, can be an important model compound to illustrate the usefulness of the present approach. Their reported experimental data are as follows: The fictitious spin-1/2 principal *g*-values are $g_1^{eff} = g_{ZZ}^{eff} = 5.79$ (corresponding to g_y^{eff} in our analysis revisited), $g_2^{eff} = g_{XX}^{eff} = 2.67$ (corresponding to g_z^{eff} in our analysis revisited), $g_3^{eff} = g_{YY}^{eff} = 3.98$ (corresponding to g_x^{eff} in our analysis revisited) and the experimental hyperfine principal values $A_1^{eff} = 603.6$ MHz, $A_2^{eff} = 58.82$ MHz and $A_3^{eff} = 167.63$ MHz, based on their

powder-pattern ESR spectral simulation. They also reported the theoretical principal values as g^{eff} = 6.29, 3.76 and 2.84 from the *ab initio* calculation for the ground Kramers doublet of complex **4**. The authors have claimed that the axial ligand field parameter Δ_{ax} is negative appearing in the Griffith Hamiltonian employed in their analysis:[18] We note that a positive Δ_{ax} gives a set of the fictitious principal *g*-values such as g_{YY}^{eff} = 5.79, g_{ZZ}^{eff} = 2.67 and g_{XX}^{eff} = 3.98 (Fig. 9 in ref. 18). In the Griffith Hamiltonian based on ligand field theory the *g*-value is considered to be isotropic and the anisotropy of the **g**-tensor comes from the effect of the orbital angular momentum operator (***L***) and the ligand field parameters.[12,65] In the Griffith Hamiltonian formalism, "the Z-axis is the axis of the low-symmetry perturbation." (p. 360 in ref. 12). We have revisited to the analysis of complex **4** in order to obtain both the principal values of the true **g**- and ZFS tensors and to check the collinearity of the two tensors. We have also attempted to carry out the DFT-based and *ab initio* quantum chemical calculations for the spin-quartet ground state of complex **4**.

We first summarize the experimental results revisited in Table 2, where the set of the principal values of the **g**- and **A**-tensors analyzed on the basis of both the fictitious-1/2 and full spin Hamiltonian approaches are given with the ZFS parameters.[11] In the spectral analyses, the collinearity of the magnetic tensors was assumed. The ZFS parameters were determined from the analysis of the documented magnetic susceptibility data combined with the experimental true *g*-values determined in this work. We have noticed that interestingly the true principal g_x- and g_y-values are close to those of the previously reported complexes, $Et_4N[Co^{II}(hfac)_3]$ with **g** = [2.448, 2.444, 2.556][51] and $[Co(acac)_2(H_2O)_2]$ with **g** = [2.50, 2.57, 2.40],[28] and the true g_z-value, g_z = 2.81 for complex **4** is significantly different.

The χT-*T* curves of complex **4** were simulated by using the set of the principal values of **g**- and **D**-tensors; the best fit the magnetic parameters are shown in Table 2, **g** = [2.50, 2.46, 2.81] and $D = +2.0 \times 10^3$ GHz (+67 cm^{-1}), *E* = 260 GHz (8.7 cm^{-1}) (*E*/*D* = 0.13) (see also Fig. S21). All these values except for g_z = 2.81 are comparable to those of the previously reported spin-quartet cobalt(II) complex $Et_4N[Co^{II}(hfac)_3]$.[51] The set of the principal values of the **A**(^{59}Co)-tensor were estimated from the spectral simulation of the powder-pattern ESR spectrum: A_x = 105.3 MHz, A_y = 256.5 MHz and A_z = 61.90 MHz (Fig. 4). They are subject to the reduction due to the influence of the spin projection factor, compared with those obtained from the fictitious spin-1/2 Hamiltonian analysis.

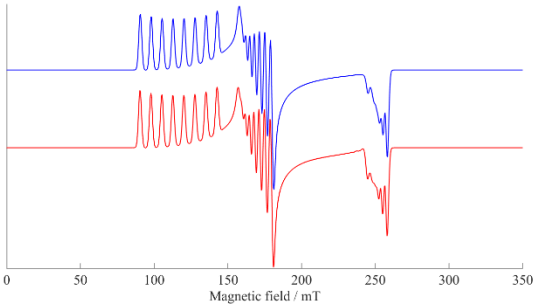

Fig. 4. The simulated randomly-oriented ESR spectra of complex **4** (*S* = 3/2) magnetically diluted in diamagnetic *cis*-$[Zn(hfac)_2(H_2O)_2]$. The spectra in blue and red are based on the fictitious spin-1/2 and ZFS + electronic Zeeman interaction spin Hamiltonian approach, respectively. Microwave frequency used: 9.4715 GHz, peak-to-peak line width: 2.0 mT. Magnetic tensors: $\mathbf{g}^{eff}$ = [5.79, 3.98, 2.67], $\mathbf{A}^{eff}(^{59}Co)$ = [603.6, 167.63, 58.82] MHz and $\mathbf{g}^{true}$ = [2.50, 2.46, 2.81], $\mathbf{A}^{true}(^{59}Co)$ = [105.3, 256.5, 61.90] MHz, $D = 2.0 \times 10^3$ GHz and *E*/*D* = 0.13. The **g**-, **A**- and **D**-tensors were assumed to be collinear. Any strain effect of the tensor and the linewidth is not included. The simulated spectra were obtained by using EasySpin (ver. 5.1.12).[34]

Table 2. The principal values of the magnetic tensors of the Co(II) complex **4** (*S*=3/2) magnetically diluted in the diamagnetic *cis*-$[Zn(hfac)_2(H_2O)_2]$ host lattice. The columns denoted by "true" and "effective" give the values based on the rank-2 ZFS + electronic Zeeman interaction Hamiltonian and fictitious spin-1/2 Hamiltonian approaches, respectively.

	True	Effective[$]
g_x	2.46	5.79 (g_{ZZ} in ref. 17)
g_y	2.50	3.98 (g_{YY} in ref. 17)
g_z	2.81	2.67 (g_{XX} in ref. 17)
$A_x(^{59}Co)$/MHz	256.5	603.6
$A_y(^{59}Co)$/MHz	105.3	167.63
$A_z(^{59}Co)$/MHz	61.90	58.82
D/cm^{-1}	+67	Not available
|*E*/*D*|	0.13	Not available

[$] Note that the definitions for the principal axes, *x*, *y* and *z* are different from those given in ref. 18.

Figure 4 shows that there is no apparent difference between the two simulated spectra because the *D*-value (*D* > 0) is large and no off-axis extra peaks due to sizable anisotropy of the g- and **D**-tensors nor the **g**- and **A**-tensors are expected to appear. Note that the principal axes corresponding to the reported g_1 (g_{XX}), g_2 (g_{YY}) and g_3 (g_{ZZ})-value[18] are defined as the principal *z*-, *y*- and *x*-axis in this work, respectively.

The ESR spectral simulation based on the full spin Hamiltonian approach gives the true **A**-tensor under the assumption of the collinearity between the magnetic tensors in the present study. The ratios between the fictitious spin-1/2 and true principal values of the **g**-tensor can afford to convert the principal values of the effective **A**(^{59}Co)-tensor to those of the true **A**(^{59}Co)-tensor[28] in the following:

603.6 MHz ÷ (5.79/2.46) = 256.5 MHz for the principal *x*-axis of the true **A**(^{59}Co)-tensor,

167.63 MHz ÷ (3.98/2.50) = 105.3 MHz for the principal *y*-axis of the true **A**(^{59}Co)-tensor and

58.82 MHz ÷ (2.67/2.81) = 61.90 MHz for the principal *z*-axis of the true **A**(^{59}Co)-tensor.

It should be noted that the above conversion implicitly includes the influence of the projection factors of the spin multiplicities.

Complex **4** is of nearly axial symmetry in terms of the experimental true **g**-tensor, but the asymmetry of the ZFS tensor is quite sizable ($|E/D|$ = 0.13). This contrasts to the case of four ligand-coordinated Co(II)octaethylporphyrin (Co^{II}OEP, S = 3/2) in tetragonal symmetry, whose magnetic property features in all the principal true g-values markedly smaller than 2.0023 (negative **g**-shift).[11] Interestingly, complex **4** is a counterpart model for an extreme case, whose true principal g-values are much larger than 2.0023. Thus, quantum chemical calculations of the magnetic tensors of complex **4** are of particular importance. The calculations were performed by using the CASSCF method. The obtained theoretical **g**-tensor is **g** = [2.147, 2.366, 2.635], revealing that the present theoretical approach tends to underestimate the positive **g**-shift from the free spin g-factor, 2.0023. We have noticed that for Co^{II}OEP the observed negative **g**-shift is underestimated, requiring theoretical improvement.[11] According to the CASSCF wavefunction, the second and third ^{4}A states (the lowest and second excited states) are mainly responsible for the g_z and g_y shift, respectively. The excitation energies of the 2 ^{4}A and 3 ^{4}A states are 1649 cm^{-1} and 2149 cm^{-1}, respectively, and we expect that excitation energies are overestimated in the CASSCF method. In fact, the MRMP2 excitation energies of the 2 ^{4}A and 3 ^{4}A states are 1460 cm^{-1} and 700 cm^{-1}, respectively, and if the CASSCF energies in the denominator of the sum-over-states (SOS) equation are replaced by the MRMP2 ones, the **g**-shifts totally increase, affording **g** = [2.119, 3.010, 2.815]. The calculated D^{SO}-value is +75.44 cm^{-1} and E^{SO}/D^{SO} = 0.325. Importantly, we have noticed that the calculated D_z principal axis is approximately parallel to the g_x axis, which is the direction along the bisector of the two Co–water coordination bonds. In the current analysis of the powder-pattern ESR spectra of complex **4**, the collinearity of the **g**- and ZFS tensors is assumed and thus the present theoretical calculations fail to reproduce the experimental findings in a quantitative manner. We emphasize that the identification of the principal axes is crucial for understanding the electronic structure of complex **4** and single crystal ESR studies of complex **4** can afford a clue because the ratio of E/D is appreciable. From the theoretical side, DFT-based approaches break down for the case of the d^7 configuration in octahedral symmetry with six ligands, failing to describe its electron ground state. On the other hand, the current stage CASSCF approach does not allow to corporate inner-shell polarization effects and only affords quantitatively poor results of the hyperfine coupling tensors of ^{59}Co nucleus in complex **4**.

This disagreement on the axis identification has urged us to check our theoretical calculations. The excited states analysis revealed that 2 ^{4}A and 3 ^{4}A states dominantly contribute to the $\mathbf{D}^{SO}$-tensor, while the contributions from the excited doublet states are small compared with those from the excited quartet states. The excitation energy of the lowest excited doublet state is 5022 cm^{-1}, and this excited state contributes positively to the D_y principal value. In the present calculations we adopted the state-specific approach for the CASSCF calculation, and therefore the descriptions of the excited states may be poor, compared with the ground state description. We also performed the $\mathbf{D}^{SO}$-tensor calculations with the state-averaged CASSCF wavefunction, but in this case the excitation energy of the 1 ^{2}A state was calculated to be 74 cm^{-1} at the MRMP2 level, which is too small to adopt the perturbation theory for the $\mathbf{D}^{SO}$-tensor calculations. Theoretical calculations with larger active space including coordinating lone pair orbitals of ligands may improve the theoretical magnetic tensors, which is out of scope of this work.

Referred to the discrepancy between the experimental and theoretical principal axes described above, we have attempted to relax the assumption of the collinearity between the magnetic tensors, applying the generalized analytical method for g^{eff}/g^{true} relationships as derived in this work and checking the breakdown of the collinearity. This gives an alternative solution to interpret the discrepancy, noting that a single crystal ESR spectroscopy of complex **4** gives a clue from the experimental side. Here, we have simulated the ESR spectra in the non-collinear case. According to the theoretical calculation, a set of the rotation angles (Euler angles) of the **g**-tensor with respect to the **D**-tensor were fixed to 0, 90 and 138 degrees, under whose condition the original principal axes of the **g**-tensor were rotated around the z, y and z-axes of the principal axes the **D**-tensor, respectively. The **A**-tensor was collinear with the **D**-tensor. We have selected one of the possible sets of the magnetic tensors, summarized in Table 3 and the simulated spectrum obtained under this choice is shown in Fig. 5 (red line). Importantly, in the collinear case, the g_z-value was larger than the g_x or g_y-value, while in the non-collinear case, the g_z-value was smaller than the g_x or g_y-value, as shown in Fig. 6. The principal z-axis of the **g**-tensor was parallel to the X-axis of the molecular coordinate axis, the bisector of the two bonds between the cobalt and oxygen atoms of water.

Table 3. The principal values of the magnetic tensors of the Co(II) complex **4** (S = 3/2) magnetically diluted in the diamagnetic *cis*-$[Zn(hfac)_2(H_2O)_2]$ host lattice in the non-collinear case.

	True
g_x	2.7
g_y	2.75
g_z	2.25
$A_x(^{59}Co)$/MHz	99.2
$A_y(^{59}Co)$/MHz	264.6
$A_z(^{59}Co)$/MHz	61.0
D/cm^{-1}	+67
E/D	0.10

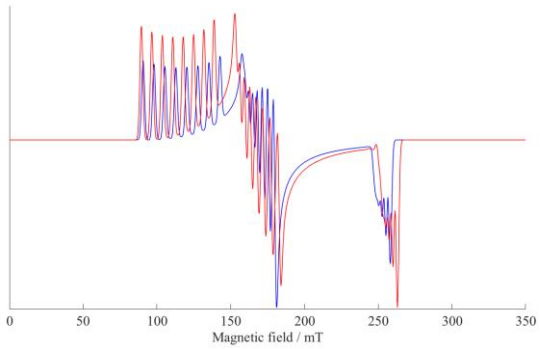

Fig. 5. The simulated powder-pattern ESR spectra of complex **4** (S = 3/2) magnetically diluted in diamagnetic *cis*-[Zn(hfac)$_2$(H$_2$O)$_2$]. The spectra in blue and red are based on the fictitious spin-1/2 and ZFS + electronic Zeeman interaction spin Hamiltonian approaches, respectively. Microwave frequency used: 9.4715 GHz, peak-to-peak line width: 2.0 mT. Magnetic tensors: $\mathbf{g}^{eff}$ = [5.79, 2.67, 3.98], $\mathbf{A}^{eff}(^{59}Co)$ = [603.6, 58.82, 167.63] MHz and $\mathbf{g}^{true}$ = [2.7, 2.75, 2.25], $\mathbf{A}^{true}(^{59}Co)$ = [99.2, 264.6, 61.0] MHz, D = +2.0 × 10^3 GHz and E/D = 0.10. The **A**- and **D**-tensors were assumed to be collinear, while the **g**-tensor was rotated 0, 90 and 138 degrees (in Euler angles) with respect to the **D**-tensor. Any strain effect of the tensor and the linewidth were not included. The simulated spectra were obtained by using EasySpin (ver. 5.1.12).[34]

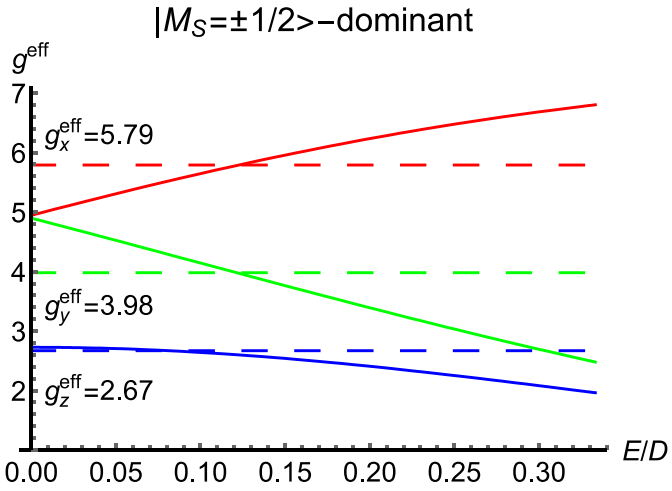

Fig. 6. The relationships of the g^{eff} and g^{true}-values calculated with the exact eigenenergies in the non-collinear case for complex **4** (S = 3/2). The solid curves were the calculated effective g-values from the true g-values (g_x = 2.7, g_y = 2.75 and g_z = 2.25) as a function of E/D for each axis. The E/D ratio used in the simulated spectrum (red line in Fig. 5) was obtained as the crossing point between the solid and the dashed lines corresponding to the principal axis. The g_x^{eff} and g_y^{eff} curves give E/D = 0.12 for the crossing points, and the g_z^{eff} one E/D = 0.10. Note that the experimental error for the ratio of E/D was estimated to be ±0.02. The experimental effective g-values (5.79, 3.98 and 2.67) denoted by the dashed lines were reported in ref. 18.

Conclusions

This work dealt with the analyses of the magnetic tensors of high spin (S = 3/2, 5/2) metallocomplexes having sizable ZFS tensors, establishing an easy-to-access approach to determine their true experimental **g**-, **A**- and rank-2 ZFS tensors in the full spin Hamiltonian, with which quantum chemical calculations can be compared, instead of the putative fictitious spin-1/2 approaches without explicitly providing the ZFS tensors. The present work gives more generalized analytical formulas for the g^{eff}/g^{true} relationships without the limitation of the collinearity between the **g**- and ZFS tensors, and the expressions are derived in two schemes; one is exact and the other is based on the genuine Zeeman perturbation treatment to the third order. All the analytical expressions are given in the principal coordinate axis systems, and thus the canonical peaks appearing in the powder-pattern fine-structure/hyperfine spectra characteristic of sizable ZFS tensors in the conventional ESR spectroscopy can easily be identified. Importantly, this spectral assignment procedure discriminates between the canonical and off-principal axis extra peaks, and the off-axis extra ones can afford to experimentally determine the accurate principal values of sizable ZFS tensors in the full spin Hamiltonian.

To illustrate the usefulness of the present analytical approach, two picket fence Mn(II)porphyrins (denoted by complex **1** and **2** in this work)[16] and 6th ligand coordinated Fe(III)porphyrin (complex **3**$^+$)[17] as important models for S = 5/2 and a *cis*-[Co(II)(hfac)$_2$(H$_2$O)$_2$] complex (complex **4**)[18] for S = 3/2 have been chosen and the analyses of their ESR spectra and magnetic susceptibility measurements revisited to carry out the complete analyses, deriving their true magnetic tensors in terms of the full spin Hamiltonian. We emphasize that there have been many peaks in the documented spectra but overlooked in terms of the spectral analyses, resulting in a complete lack of the important information on the ZFS tensors of the metalloporphyrins (complex **1** and **2**). The observed peaks are fully assigned to the off-axis extra peaks, affording the accurate magnetic tensors of the metalloporphyrins (complex **1** and **2**). By using the g^{eff}/g^{true} relationship, we have determined for the first time the experimental true **g**-, **A**- and rank-2 ZFS tensors of the picket fence Mn(II)porphyrins (complex **1** and **2**) and 6th ligand coordinated Fe(III)porphyrin (complex **3**$^+$) and compared with the theoretical tensors acquired by reliable quantum chemical calculations with our lab-coded software. The quantum chemical calculations have reasonably well reproduced the experimental true magnetic tensors, affording to interpret the detailed electronic structures in terms the magnetic tensors.

The picket fence Mn(II)porphyrins (S = 5/2) with the planar porphyrin skeleton feature in relatively small positive D-values (~ 0.7 cm^{-1}) and nearly axial symmetry of the ZFS tensors. On the other hand, the 6th ligand coordinated Fe(III)porphyrin (complex **3**$^+$), which also has the planar skeleton with the nearly axial symmetry of the ZFS tensor, is characterized by a positive D-value as large as a few to 10 cm^{-1}. The sizable D-value is a comparable figure for Fe(III)(Cl)octaethlporphyrin with the ruffled porphyrin skeleton[11] and other hemoproteins. The experimental true **g**-tensor of **3**$^+$ is isotropic and all the principal g-values are very close to and less than 2.0023.

For complex **4**, *cis*-[Co^{II}(hfac)$_2$(H$_2$O)$_2$] magnetically diluted in the host metallocomplex, *cis*-[Zn(hfac)$_2$(H$_2$O)$_2$], the principal values of the true **g**- and **A**(^{59}Co)-tensor are [2.46, 2.50, 2.81] (g_{iso} = 2.59) and [256.5, 105.3, 61.90] MHz (A_{iso} = 141.2 MHz) and the D- and E-values are +2.0 × 10^3 GHz (= +67 cm^{-1}), 260 GHz (= 8.7 cm^{-1}) (E/D = 0.13), respectively, assuming the collinearity between the magnetic tensors. The theoretical interpretations for the true experimental magnetic tensors were performed by using the CASSCF and the hybrid

CASSCF/MRMP2 method. The obtained theoretical **g**-tensor is **g** = [2.147, 2.366, 2.635], revealing that the present theoretical approach tends to underestimate the positive **g**-shift from the free spin *g*-factor, 2.0023, as a similar underestimation revealed for the case of the negative **g**-shift such as four-ligand-coordinated Co^{II}octaethylporphyrin with the ruffled structure of the porphyrin skeleton.[11] We have attempted to apply the present generalized approach for the g^{eff}/g^{true} relationships to experimentally derive the true magnetic tensors of complex **4** with a sizable *D*-value and significant non-axial property of the ZFS tensors, interpreting the complex electronic structure in terms of the quantum chemical calculations instead of ligand field theory. We note that in order to settle the issue of the non-collinearity in complex **4** the single crystal ESR spectroscopy at X- or Q-band will give a clue.

In quest of new magnetic functionalities of synthetic open shell metallocomplexes and in emerging fields such as implementation of molecular-spin qubit based quantum computers and quantum spin memory devices, it is important to evaluate true ZFS tensors, as governed by spin–orbit couplings, whose magnitude ranges from a few tenths to hundreds of cm^{-1}. The present approaches are experimentally underlain by conventional ESR spectroscopy at X- or Q-band, attempting to strengthen the spectroscopy. We also emphasize that sophisticated high-field/high-frequency ESR measurements afford the determination of sizable ZFS values in a straightforward manner. The approaches given in this work are in good harmony with any results from the high-field/high-frequency ESR spectroscopy, particularly because the exact analytical approach is free from the magnitude of the magnetic field and frequency used in ESR experiments. All the derived formulas are analytical and easy-to-access, comparing experimental true tensors with quantum chemical theoretical counterparts and thus giving physical insights in a rather straightforward manner.

Conflicts of interest

There are no conflicts to declare.

Acknowledgments

This work was supported by AOARD Scientific Project on "Quantum Properties of Molecular Nanomagnets" (Award No. FA2386-13-4029, 13-4030, 13-4031) and the AOARD Project on “Molecular Spins for Quantum Technologies” (Grant No. FA2386-17-1-4040). The support by JSPS Grants-in-Aid for Scientific Research (B) and (C) 26400400 and 26400422 from Ministry of Education, Culture, Sports, Science and Technology (Japan) is acknowledged. The support by JSPS KAKENHI Grant Numbers 17H03012, 17K05840 and 18K03465 is also acknowledged. The work was partially supported by Grants-in-Aid for Scientific Research on Innovative Areas (Quantum Cybernetics), Scientific Research (B) (No. 23350011), Grants-in-Aid for Challenging Exploratory Research (No. 25620063) from the Ministry of Education, Culture, Sports, Science and Technology (the MEXT, Japan), and also by FIRST Quantum Information Processing Project, Cabinet Office, Government of Japan and by by Open Advanced Research Facilities Initiative Program from the MEXT, Japan.

References

1 D. Dolphin ed., *The Porphyrins*, Academic Press, New York, 1978, 1979.
2 B. J. Gaffney and H. J. Silverstone, Simulation of the EMR Spectra of High-Spin Iron in Proteins, in *Biological Magnetic Resonance*, eds., L. Berliener and J. Reuben, Plenum Press, 1993, **13**, 1–57.
3 B. J. Gaffney, EPR of Mononuclear Non-Heme Iron Proteins, in *Biological Magnetic Resonance*, eds. G. Hanson, L. Berliener, Splinger, 2009, **28**, 233–268.
4 C. Bonizzoni, A. Ghirri and M. Affronte, Coherent Coupling of Molecular Spins with Microwave Photons in Planar Superconducting Resonators, *Advances in Physics: X*, 2018, **3**, 1435305.
5 C. Bonizzoni, F. Troiani, A. Ghirri and M. Affronte, Microwave Dual-Mode Resonators for Coherent Spin-Photon Coupling, arXiv: 1805.05843.
6 W. C. Lin, Electron Spin Resonance and Electronic Structure of Metalloporphyrins, in Ref. 1, 1979, 355–377.
7 W. C. Lin, Further Work on the Calculation of d-Orbital Energies of Cobalt Porphyrins from Electron Spin Resonance Data, *Inorg. Chem.*, 1980, **19**, 1072–1073.
8 J. Kortus, T. Baruah, N. Bernstein and M. R. Pederson, Magnetic Ordering, Electronic Structure, and Magnetic Anisotropy Energy in the High-Spin Mn_{10} Single Molecule Magnet, *Phys. Rev. B*, 2002, **66**, 092403.
9 C. van Wullen, Broken Symmetry Approach to Density Functional Calculation of Magnetic Anisotropy or Zero Field Splittings for Multinuclear Complexes with Antiferromagnetic Coupling, *J. Phys. Chem. A*, 2009, **113**, 11535‑11540.
10 S. Sano, T. Kawakami, S. Yoshimura, M. Shoji, S. Yamanaka, M. Okumura, T. Nakajima and K. Yamaguchi, Ab initio Computations of Zero-Field Splitting Parameters and Effective Exchange Integrals for Single-Molecule Magnets (Mn_{12}- and Mn_{11}Cr-acetate Clusters), *Polyhedron*, 2017, **136**, 159‑169.
11 T. Yamane, K. Sugisaki, T. Nakagawa, H. Matsuoka, T. Nishio, S. Kinjyo, N. Mori, S. Yokoyama, C. Kawashima, N. Yokokura, K. Sato, Y. Kanzaki, D. Shiomi, K. Toyota, D. H. Dolphin, W.-C. Lin, C. A. McDowell, M. Tadokoro and T. Takui, Analyses of Sizable ZFS and Magnetic Tensors of High Spin Metallocomplexes, *Phys. Chem. Chem. Phys.*, 2017, **19**, 24769–24791.
12 J. S. Griffith, *The Theory of Transition-Metal Ions,* University Press, Cambridge, U. K., 1964.
13 M. Zerner and M. Gouterman, Porphyrins, Porphyrins IV. Extended Hückel Calculations on Transition Metal Complexes, *Theoret. Chim. Acta*, 1966 **4**, 44–63.
14 M. Zerner, M. Gouterman and H. Kobayashi, Porphyrins VIII. Extended Hückel Calculations on Iron Complexes, *Theoret. Chim. Acta*, 1966 **6**, 363–400.
15 B. R. McGarvey, The Isotropic Hyperfine Interaction, *J. Phys. Chem.*, 1967, **71**, 51–66.
16 Q. Yu, Y. Liu, D. Liua and J. Li, Geometric and Electronic Structures of Five-Coordinate Manganese(II) “Picket Fence” Porphyrin Complexes, *Dalton Trans.*, 2015, **44**, 9382–9390.
17 Y. Ide, N. Murai, H. Ishimae, M. Suzuki, S. Mori, M. Takahashi, M. Nakamura, K. Yoshino and T. Ikeue, Spin-Crossover between High-Spin (S = 5/2) and Low-Spin (S = 1/2) States in Six-Coordinate Iron(III) Porphyrin Complexes Having Two Pyridine-N Oxide Derivatives, *Dalton Trans.*, 2017, **46**, 242–249.

18 D. V. Korchagin, A. V. Palii, E. A. Yureva, A. V. Akimov, E. Ya. Misochko, G. V. Shilov, A. D. Talantsev, R. B. Morgunov, A. A. Shakin, S. M. Aldoshin and B. S. Tsukerblat, Evidence of Field Induced Slow Magnetic Relaxation in *cis*-$[Co(hfac)_2(H_2O)_2]$ Exhibiting Tri-Axial Anisotropy with a Negative Axial Component, *Dalton Trans.*, 2017, **46**, 7540−7548.

19 K. Sugisaki, K. Toyota, K. Sato, D. Shiomi and T. Takui, Ab Initio MO Analysis of the Excited Electronic States of High-Spin Quintet 2-Methylphenylene-1,3-dinitrene, *Angew. Chem. Int. Ed.*, 2006, **45**, 2257–2260.

20 K. Sugisaki, K. Toyota, K. Sato, D. Shiomi, M. Kitagawa and T. Takui, *Ab initio* Calculations of Spin–Orbit Contribution to the Zero-Field Splitting Tensors of $n\pi^*$ Excited States by the CASSCF Method with MRMP2 Energy Correction, *Chem. Phys. Lett.*, 2009, **477**, 369–373.

21 K. Sugisaki, K. Toyota, K. Sato, D. Shiomi, M. Kitagawa and T. Takui, Spin-Orbit Contributions in High-Spin Nitrenes/Carbenes: A Hybrid CASSCF/MRMP2 Study of Zero-Field Splitting Tensors, *ChemPhysChem*, 2010, **11**, 3146–3151.

22 K. Sugisaki, K. Toyota, K. Sato, D. Shiomi, M. Kitagawa and T. Takui, Ab initio and DFT Studies of the Spin–Orbit and Spin–Spin Contributions to the Zero-Field Splitting Tensors of Triplet Nitrenes with Aryl Scaffolds, *Phys. Chem. Chem. Phys.*, 2011, **13**, 6970–6980.

23 K. Sugisaki, K. Toyota, K. Sato, D. Shiomi, M. Kitagawa and T. Takui, An Ab initio MO Study of Heavy Atom Effects on the Zero-Field Splitting Tensors of High-Spin Nitrenes: How the Spin–Orbit Contributions are Affected, *Phys. Chem. Chem. Phys.*, 2014, **16**, 9171–9181.

24 K. Sugisaki, K. Toyota, K. Sato, D. Shiomi and T. Takui, Quasi-Restricted Orbital Treatment for the Density Functional Theory Calculations of the Spin–Orbit Term of Zero-Field Splitting Tensors, *J. Phys. Chem. A*, 2016, **120**, 9857–9866.

25 K. Sugisaki, K. Toyota, K. Sato, D. Shiomi and T. Takui Behaviour of DFT-Based Approaches to the Spin–Orbit Term of Zero-Field Splitting Tensors: A Case Study of Metallocomplexes, $M^{III}(acac)_3$ (M = V, Cr, Mn, Fe and Mo), *Phys. Chem. Chem. Phys.*, 2017, **19**, 30128−30138.

26 T. Takui, S. Nakazawa, H. Matsuoka, K. Furukawa, K. Sato and D. Shiomi, Molecule-Based Exchange-Coupled High-Spin Clusters: Conventional, High-Field/High-Frequency and Pulse-Based Electron Spin Resonance of Molecule-Based Magnetically Coupled Systems, In *EPR of Free Radicals in Solids II*, eds. A. Lund and M. Shiotani, Springer, 2003, pp. 71−162.

27 E. Bartolomé, P. J. Alonso, A. Arauzo, J. Luzón, J. Bartolomé, C. Racles and C. Turta, Magnetic Properties of the Seven-Coordinated Nanoporous Framework Material $Co(bpy)_{1.5}(NO_3)_2$ (bpy = 4,4′-bipyridine), *Dalton Trans.*, 2012, **41**, 10382–10389.

28 S. Gómez-Coca, A. Urtizberea, E. Cremades, P. J. Alonso, A. Camón, E. Ruiz and F. Luis, Origin of Slow Magnetic Relaxation in Kramers Ions with Non-Uniaxial Anisotropy, *Nat. Commun.*, 2014, **5**, 4300.

29 B. Bleaney and K. D. Bowers, Anomalous Paramagnetism of Copper Acetate, *Proc. Roy. Soc. A*, 1952, **214**, 451−465.

30 J. W. Orton, *Paramagnetic Resonance: An Introduction to Transition Group Ions in Crystals*, Gordon and Breach, 1968.

31 C. Rudowicz and R. Bramley, On Standardization of the Spin Hamiltonian and the Ligand Field Hamiltonian for Orthorhombic Symmetry, *J. Chem. Phys.*, 1985, **83**, 5192−5197.

32 R. Kripal, D. Yadav, P. Gnutek and C. Rudowicz, Alternative Zero-Field Splitting (ZFS) Parameter Sets and Standardization for Mn^{2+} ions in various Hosts Exhibiting Orthorhombic Site Symmetry, *J. Phys. Chem. Solids*, 2009, **70**, 827−833.

33 F. Klein, *Lectures on the Icosahedron and the Solution of the Fifth Degree* (*English translation*), Cosimo Classics Inc., 2007.

34 S. Stoll and A. Schweiger, EasySpin, a Comprehensive Software Package for Spectral Simulation and Analysis in EPR, *J. Magn. Reson.*, 2006, **178**, 42−55.

35 F. Neese, The ORCA Program System, *Wiley Interdiscip. Rev.: Comput. Mol. Sci.*, 2012, **2**, 73−78.

36 M. W. Schmidt, K. K. Baldridge, J. A. Boatz, S. T. Elbert, M. S. Gordon, J. H. Jensen, S. Koski, N. Matsunaga, K. A. Nguyen, S. J. Su, T. L. Windus, N. Dupis and J. A. Montgomery, General Atomic and Molecular Electronic Structure System, *J. Comput. Chem.*, 1993, **14**, 1347−1363.

37 Y.-K. Choe, H. A. Witek, J. P. Finley and K. Hirao, Intruder State Avoidance Multireference Møller–Plesset Perturbation Theory, *J. Comput. Chem.*, 2002, **23**, 957–965.

38 K. M. Kadish, K. M. Smith and R. Guilard eds., *Porphyrin Handbook*, Academic Press, 1999.

39 J. Hütterman and R. Kappl, ENDOR: Probing the Coordination Environment in Metalloproteins, in *Metal Ions in Biological Systems*, ed. H. Sigel, Marcel Dekker, Inc., 1987, **22**, 1–80.

40 C. P. Scholes, ENDOR on Hemes and Hemoproteins, in *Multiple Electron Resonance Spectroscopy*, eds. M. M. Dorio and J. H. Freed, Springer, Boston, MA, 1979, 297–329.

41 S. K. Misra, H. A. Buckmaster, E. Reijerse, S. Subramanian and M. C. Krishna, Spectrometers, in *Multifrequency Electron Paramagnetic Resonance: Theory and Applications*, ed. S. K. Misra, Wiley-VCH, 2011, 115–228.

42 F. A. Walker and U. Simonis, Iron Porphyrin Chemistry, in *Encyclopedia of Inorganic and Bioinorganic Chemistry*, ed. R. A. Scott, John Wiley & Sons, 2011.

43 J. P. Collman, R. R. Gagne, C. A. Reed, T. R. Halbert, G. Lang and W. T. Robinson, "Picket Fence Porphyrins." Synthetic Models for Oxygen Binding Hemoproteins, *J. Am. Chem. Soc.*, 1975, **97**, 1427−1439.

44 J. P. Collman, J. I. Brauman and K. S. Suslick, Oxygen Binding to Iron Porphyrins, *J. Am. Chem. Soc.*, 1975, **97**, 7185−7186.

45 J. F. Kirner, C. A. Reed and W. R. Scheidt, Stereochemistry of Manganese Porphyrins. 3. Molecular Stereochemistry of α,β,γ,δ-Tetraphenylporphinato-(1-methylimidazole)manganese(II), *J. Am. Chem. Soc.*, 1977, **99**, 2557−2563.

46 C. G. Howard, G. S. Girolami, G. Wilkinson, M. Thornton-Pett and M. B. Hursthouse, Tertiary Phosphine Adducts of Manganese(II) Dialkjyls. Part 2. Synthesis, Properties, and Structures of Monomeric Complexes, *J. Chem. Soc., Dalton Trans.*, 1983, 2631.

47 M. He, X. Li, Y. Liu and J. Li, Axial Mn-C_{CN} Bonds of Cyano Manganese(II) Porphyrin Complexes: Flexible or Weak? *Inorg. Chem.*, 2016, **55**, 5871−5879.

48 T. Koto, K. Sato, D. Shiomi, K. Toyota, K. Itoh, E. Wassermann and T. Takui, Random-Orientation High-Spin Electron Spin Resonance Spectroscopy and Comprehensive Spectral Analyses of the Quintet Dicarbene and Dinitrene with *meta*-Topological Linkers: Origins of Peculiar Line-Broadening in Fine-Structure ESR Spectra in Organic Rigid Glasses, *J. Phys. Chem. A*, 2009, **113**, 9521−9526.

49 T. Koto, K. Sugisaki, K. Sato, D. Shiomi, K. Toyota, K. Itoh, E. Wassermann, P. M. Lahti and T. Takui, High-Spin Nitrene Fine-Structure ESR Spectroscopy in Frozen Rigid Glasses: Exact Analytical Expressions for the Canonical Peaks and a D-Tensor Gradient Method for Line Broadening, *Appl. Magn. Reson.*, 2010, **37**, 703–736.

50 S. Nakazawa, T. Kanno, K. Sugisaki, H. Kameya, M. Matsui, M. Ukai, K. Sato and T. Takui, Fe-Transferrins or their Homologues in ex-vivo Mushrooms as Identified by ESR Spectroscopy and Quantum Chemical Calculations: A Full Spin-Hamiltonian Approach for the Ferric Sextet State with Intermediate Zero-Field Splitting Parameters, *Food Chemistry*, 2018, **266**, 24–30.

51 R. Patra, S. Bhowmik, S. K. Ghosh and S. P. Rath, Effects of Axial Pyridine Coordination on a Saddle-Distorted Porphyrin Macrocycle: Stabilization of Hexa-Coordinated High-Spin Fe(III) and Air-Stable Low-Spin Iron(II) Porphyrinates, *Dalton Trans.*, 2010, **39**, 5795–5806.

52 A. V. Palii, D.V. Korchagin, E. A. Yureva, A. V. Akimov, E. Ya. Misochko, G. V. Shilov, A. D. Talantsev, R. B. Morgunov, S. M. Aldoshin and B. S. Tsukerblat, Single-Ion Magnet $Et_4N[Co^{II}(hfac)_3]$ with Nonuniaxial Anisotropy: Synthesis, Experimental Characterization, and Theoretical Modeling, *Inorg. Chem.*, 2016, **55**, 9696−9706.

53 R. Ishikawa, Y. Horii, R. Nakanishi, S. Ueno, B. K. Breedlove, M. Yamashita and S. Kawata, Field-Induced Single-Ion Magnetism Based on Single-Phonon Relaxation in a Distorted Octahedral High-Spin Cobalt(II) Complex, *Eur. J. Inorg. Chem.*, 2016, **2016**, 3233−3239.

54 R. Herchel, L. Váhovská, I. Potočňák and Z. Trávníček, Slow Magnetic Relaxation in Octahedral Cobalt(II) Field-Induced Single-Ion Magnet with Positive Axial and Large Rhombic Anisotropy, *Inorg. Chem.*, 2014, **53**, 5896−5898.

55 Y. Y. Zhu, M. S. Zhu, T. T. Yin, Y. S. Meng, Z. Q. Wu, Y. Q. Zhang and S. Gao, Cobalt(II) Coordination Polymer Exhibiting Single-Ion-Magnet-Type Field-Induced Slow Relaxation Behavior, *Inorg. Chem.*, 2015, **54**, 3716−3718.

56 J. P. S. Walsh, G. Bowling, A.-M. Ariciu, N. F. M. Jailani, N. F. Chilton, P. G. Waddell, D. Collison, F. Tuna and L. J. Higham, Evidence of Slow Magnetic Relaxation in $Co(AcO)_2(py)_2(H_2O)_2$, *Magnetochemistry*, 2016, **2**, 23−33.

57 A. Świtlicka-Olszewska, J. Palion-Gazda, T. Klemens, B. Machura, J. Vallejo, J. Cano, F. Lloret and M. Julve, Single-Ion Magnet Behaviour in Mononuclear and Two-Dimensional Dicyanamide-Containing Cobalt(II) Complexes, *Dalton Trans.*, 2016, **45**, 10181−10193.

58 J. Vallejo, I. Castro, R. Ruiz-García, J. Cano, M. Julve, F. Lloret, G. De Munno, W. Wernsdorfer and E. Pardo, Field-Induced Slow Magnetic Relaxation in a Six-Coordinate Mononuclear Cobalt(II) Complex with a Positive Anisotropy, *J. Am. Chem. Soc.*, 2012, **134**, 15704−15707.

59 J. Palion-Gazda, T. Klemens, B. Machura, J. Vallejo, F. Lloret and M. Julve, M. Single Ion Magnet Behaviour in a Two-Dimensional Network of Dicyanamide-Bridged Cobalt(II) Ions, *Dalton Trans.*, 2015, **44**, 2989−2992.

60 C. Plenk, J. Krause and E. Rentschler, A Click-Functionalized Single-Molecule Magnet Based on Cobalt(II) and its Analogous Manganese(II) and Zinc(II) Compounds, *Eur. J. Inorg. Chem.*, 2015, **2015**, 370−374.

61 X. Liu, L. Sun, H. Zhou, P. Cen, X. Jin, G. Xie, S. Chen and Q. Hu, Single-Ion-Magnet Behavior in a Two-Dimensional Coordination Polymer Constructed from Co^{II} Nodes and a Pyridylhydrazone Derivative, *Inorg. Chem.*, 2015, **54**, 8884−8886.

62 Y. Rechkemmer F. D. Breitgoff, M. van der Meer, M. Atanasov, M. Hakl, M. Orlita, P. Neugebauer, F. Neese, B. Sarkar and J. van Slageren, A Four-Coordinate Cobalt(II) Single-Ion Magnet with Coercivity and a Very High Energy Barrier, *Nat. Commun.*, 2016, **7**, 10467.

63 G. Novitchi, S. Jiang, S. Shova, F. Rida, I. Hlavička, M. Orlita, W. Wernsdorfer, R. Hamze, C. Martins, N. Suaud, N.; Guihéry, A.-L. Barra and C. Train, From Positive to Negative Zero-Field Splitting in a Series of Strongly Magnetically Anisotropic Mononuclear Metal Complexes, *Inorg. Chem.*, 2017, **56**, 14809–14822.

64 E. A. Buvaylo, V. N. Kokozay, O. Yu. Vassilyeva, B. Skelton, A. Ozarowski, J. Titiš, B. Vranovičová and R. Boča, Field-Assisted Slow Magnetic Relaxation in a Six-Coordinate Co(II)–Co(III) Complex with Large Negative Anisotropy, *Inorg. Chem.*, 2017, **56**, 6999–7009.

65 O. Kahn, *Molecular Magnetism*, VCH Publications, New York, 1993.